Biophysical Journal
Article

Biophysical Society

Thermodynamic Modeling of the Statistics of Cell Spreading on Ligand-Coated Elastic Substrates

Eoin McEvoy,[1] Siamak S. Shishvan,[2,3] Vikram S. Deshpande,[3] and J. Patrick McGarry[1,*]
[1]College of Engineering and Informatics, National University of Ireland Galway, Galway, Republic of Ireland; [2]Department of Structural Engineering, University of Tabriz, Tabriz, East Azarbayjan, Iran; and [3]Department of Engineering, University of Cambridge, Cambridge, United Kingdom

ABSTRACT Biological spread cells exist in a perpetually fluctuating state and therefore cannot be described in terms of a unique deterministic system. For modeling approaches to provide novel insight and uncover new mechanisms that drive cell behavior, a framework is required that progresses from traditional deterministic methods (whereby simulation of an experiment predicts a single outcome). In this study, we implement a new, to our knowledge, modeling approach for the analysis of cell spreading on ligand-coated substrates, extending the framework for nonequilibrium thermodynamics of cells developed by Shishvan et al. to include active focal adhesion assembly. We demonstrate that the model correctly predicts the coupled influence of surface collagen density and substrate stiffness on cell spreading, as reported experimentally by Engler et al. Low surface collagen densities are shown to result in a high probability that cells will be restricted to low spread areas. Furthermore, elastic free energy induced by substrate deformation lowers the probability of observing a highly spread cell, and, consequentially, lower cell tractions affect the assembly of focal adhesions. Experimentally measurable observables such as cell spread area and aspect ratio can be directly postprocessed from the computed homeostatic ensemble of (several million) spread states. This allows for the prediction of mean and SDs of such experimental observables. This class of cell mechanics modeling presents a significant advance on conventional deterministic approaches.

INTRODUCTION

There is no unique outcome for tissue development in nature. For example, examination of arterial tissue across several samples reveals nonhomogenous structures with nonuniform collagen fiber alignment, tissue thickness, and smooth muscle cell (SMC) morphology (1–3). The same is true in vitro, in which cells of the same phenotype exhibit a diverse range of spread shapes, area, stress-fiber (SF) alignments, and focal adhesion (FA) distributions. However, over large populations, the statistics of observables is highly reproducible. Several experimental studies have demonstrated that the microenvironment has a significant impact on cell behavior. Jacot et al. (4) show that sarcomere development and alignment in cardiomyocytes are dependent on substrate stiffness. A study by Arnold et al. (5) reveals that FA and SF formation are limited by ligand spacing on the substrate. Engler et al. (3) show that both the mean and standard error of SMC spread area depend on substrate rigidity and ligand density; with decreasing surface collagen density and decreasing substrate stiffness, the standard error reported for the experiment reduces.

It is therefore evident that to uncover the biomechanisms underlying such observations, a statistical mechanics approach to cell modeling is required. Typically, previous models have assumed the spread state as the reference configuration and simulate a single deterministic outcome (6–12). McEvoy et al. (13) recently implemented a framework whereby an initially unadhered cell deforms to a range of possible spread states, and the system free energy is computed for each configuration. It is demonstrated that cell spreading entails a competition between the increasing elastic free energy because of the stretching of passive cell components and the decreasing cytoskeletal free energy as contractile proteins assemble to form SFs. Such a competition allows for the identification of a low free-energy state, and it is shown that the predicted cell areas and SF alignments in these configurations are similar to reported experimental measurements (14). However, in the study of McEvoy et al. (13), a single low-energy spread state is identified. This deterministic approach neglects the fact that cells display a fluctuating response to their microenvironment in terms of observables such as SF alignment and spread area.

In this study, we implement a statistical mechanics framework for the homeostatic ensemble of spread cells, following

Submitted August 13, 2018, and accepted for publication November 6, 2018.
*Correspondence: patrick.mcgarry@nuigalway.ie
Editor: Cynthia Reinhart-King.
https://doi.org/10.1016/j.bpj.2018.11.007

the approach of Shishvan et al. (15). This methodology allows for the simulation of a large collection of spread microstates the cell-substrate system assumes while maintaining its homeostatic state. The framework incorporates mathematical models to describe SF formation and cell-substrate deformation. Here, we expand the model for the calculation of Gibbs free energy to include the free energy associated with the traction-dependent FA assembly. Simulations accurately predict the dependence of cell area and shape on surface collagen density and substrate stiffness, as reported in the experimental study of Engler et al. (3).

METHODS

We aim to analyze the response of cells adhered to collagen-coated elastic substrates. This experimental system is responding to both mechanical and chemical cues from its environment, viz the stiffness of the substrate and the extracellular proteins (collagen) through which the cells adhere to the substrates. The response of this complex system is recorded through a range of observables, all of which exhibit large variations but with trends clearly emerging when the statistics of these observables are analyzed. This motivates our choice of a modeling framework, called homeostatic statistical mechanics (15), in which, just as in the experimental system, observables fluctuate, and trends (and understanding) emerge once these observables are viewed statistically. This framework has previously been shown to successfully capture a range of observations for SMCs seeded on elastic substrates in which perfect adhesion was assumed and the role of the extracellular matrix neglected. Here, we extend the framework to include an adhesion model and thus will first give a brief overview of the modeling framework (details in Supporting Materials and Methods, Section S1) and then focus on the adhesion model.

Overview of the homeostatic mechanics framework

The homeostatic mechanics framework recognizes that the cell is an open system that exchanges nutrients with the surrounding nutrient bath. These high-energy nutrient exchanges fuel fluctuations in cell responses associated with various intracellular biochemical processes (such nonthermal nutrient-fueled fluctuations are observed to be very large and occur over very long timescales, compared to conventional thermal fluctuations). However, these biochemical processes attempt to maintain the cell in a homeostatic state (i.e., the cell actively maintains its various molecular species at a specific average number over these fluctuations that is independent of the environment). This translates to the constraint on the average Gibbs free energy (16) of the cell. Employing the ansatz that biochemical processes such as actin polymerization and treadmilling provide the mechanisms to maximize the morphological entropy of the cell subject to the constraint that the cell maintains a homeostatic state, Shishvan et al. (15) obtained the distribution of states that the cell assumes in terms of the Gibbs free energy $G^{(j)}$ of the morphological state (j) of the system as follows:

$$P_{\text{eq}}^{(j)} = \frac{1}{Z}\exp\left(-\zeta G^{(j)}\right). \tag{1}$$

$Z \equiv \sum_j \exp(-\zeta G^{(j)})$ is the partition function of the morphological microstates, and the distribution parameter ζ follows from the following homeostatic constraint:

$$\frac{1}{Z}\sum_j G^{(j)}\exp\left(-\zeta G^{(j)}\right) = G_{\text{S}}\,, \tag{2}$$

where G_{S} is equal to the equilibrium Gibbs free energy of an isolated cell in suspension (free-standing cell), that is, the homeostatic processes maintain the average biochemical state of the system equal to that of a cell in suspension. Thus, the distribution (Eq. 1) is characterized by a homeostatic temperature $1/\zeta$ that is conjugated to the morphological entropy of the cell. We employ Markov Chain Monte Carlo to construct a Markov chain that is representative of the homeostatic ensemble. This involves three steps: 1) a discretization scheme to represent morphological microstate (j), 2) calculation of $G^{(j)}$ for a given morphological microstate (j), and 3) construction of a Markov chain comprising these morphological microstates. Typical Markov chains comprised in excess of 2.5 million spread states (a detailed overview of the procedure is provided in Supporting Materials and Methods, Section S2.2).

Free energy $G^{(j)}$ of a morphological state

Much like conventional statistical mechanics frameworks that require a model for the energy of molecular systems, the homeostatic statistical mechanics framework requires a model for the Gibbs free energy $G^{(j)}$ of a morphological state (j) of the system. Here, we employ a relatively simple model for the Gibbs free energy wherein the cell consists of a passive elastic nucleus within a cytoplasm that is modeled as comprising an active SF cytoskeleton and elements such as the cell membrane, intermediate filaments, and microtubules that are all lumped into a single passive-elastic contribution.

Details of the model, including the parameters used to characterize the SMCs, are given in Supporting Materials and Methods, Section S2. Here, we briefly describe the salient features of the model for SMCs on elastic substrates. The SMCs are modeled as two-dimensional bodies in the $x_1 - x_2$ plane lying on the surface of an elastic substrate such that the out-of-plane Cauchy stress $\sum_{33} = 0$. The substrates are modeled as linear elastic half spaces, whereas the cells are modeled using the approach of Vigliotti et al. (17) as modified by Shishvan et al. (15). The Vigliotti et al. (17) model assumes only two elements within the cell: 1) a passive elastic contribution from elements such as the cell membrane, intermediate filaments, and microtubules and 2) contractile actomyosin SFs that are modeled explicitly. The cell in its undeformed state is a circle of radius R_0 and, for a given morphological microstate (j), the strain distribution within the cell is specified. This directly gives the elastic strain energy of the cell $\widehat{F}_{\text{passive}}$ via a two-dimensional Ogden-type hyperelastic model for both the nucleus and cytoplasm. The passive hyperelastic behavior of the cytoplasm and nucleus has been characterized for several cell types using experimental techniques in which SFs are disrupted using Cytochalasin D (18–20). The SF cytoskeleton within the cytoplasm is modeled as a distribution of SFs such that at each location x_i within the cell $\widehat{\eta}(\varphi)$ parameterizes the angular concentration of SFs over all angles φ, whereas $\widehat{n}^{ss}(\varphi)$ denotes the number of functional units within each SF. Thus, at any x_i, there is a total concentration $\widehat{N}_{\text{b}}$ of bound SF proteins obtained by integrating $\widehat{\eta}\widehat{n}^{ss}$ over all orientations φ, and these bound proteins are in chemical equilibrium with the unbound SF proteins. The unbound proteins are free to diffuse within the cell, and thus, at equilibrium of a morphological microstate, the concentration $\widehat{N}_{\text{u}}$ of these unbound SF proteins is spatially uniform. This chemical equilibrium condition along with the conservation of SF proteins within the cell provides the spatial and angular distributions of SFs from which the free energy of the cytoskeleton $\widehat{F}_{\text{cyto}}$ is evaluated. The total normalized free energy of the cell's morphological microstate (j) then follows as $\widehat{G}^{(j)} \equiv \widehat{F}^{(j)}_{\text{passive}} + \widehat{F}^{(j)}_{\text{cyto}} + \widehat{F}^{(j)}_{\text{sub}}$, where $\widehat{F}^{(j)}_{\text{sub}}$ is the elastic energy of the substrate ($\widehat{G}^{(j)}$ is the normalized value of $G^{(j)}$; see Supporting Materials and Methods (Section S2.4) for details of the normalizations).

In addition to the contributions to $\widehat{G}^{(j)}$ from the passive elasticity and cytoskeleton of the cell, here we also include the contribution from the FAs between the cell and the collagen extracellular matrix laid on the elastic

substrates on which the SMCs are seeded. Shishvan et al. (15) implicitly assumed an unlimited supply of adhesion proteins as well as extracellular proteins to form adhesion complexes and thereby neglected the contribution of adhesion to $\widehat{G}^{(j)}$. Here, we extend the approach of Shishvan et al. (15) for the case of a finite quantity of both FA proteins and extracellular collagen and thus explicitly include an adhesion contribution to $\widehat{G}^{(j)}$; that is, we write $\widehat{G}^{(j)}$ as follows:

$$\widehat{G}^{(j)} \equiv \widehat{F}^{(j)}_{\text{passive}} + \widehat{F}^{(j)}_{\text{cyto}} + \widehat{F}^{(j)}_{\text{sub}} + \widehat{F}^{(j)}_{\text{adh}}. \tag{3}$$

We now proceed to make explicit this adhesion model.

Adhesion complexes between the cell and the extracellular collagen

The FA model proposed here is a modification to the model of McEvoy et al. (13) in which adhesion is assumed to be via integrins that exist in a single state. These integrins form complexes by binding to ligands that have a density N_{H} per unit area on the surface of the elastic substrate. For a given morphological microstate (j), the strain state of the cell is specified, and this implies that the tractions $\text{T}_i(x_i)$ that the cells exert on the substrate are also fixed from the cell model; see Supporting Materials and Methods, Section S2.1 (for the sake of brevity, here we have dropped the superscript (j) to indicate that these are tractions for a given morphological microstate (j)). These tractions are transmitted to the substrate through the FA complexes, and here we explain the adhesion model with the tractions $\text{T}_i(x_i)$ specified.

When in local equilibrium at a location x_i on the surface of the cell, the integrins with a local concentration $C_{\text{I}}(x_i)$ have a chemical potential at temperature T in terms of the Boltzmann constant k_{B}:

$$\chi_{\text{I}}(x_i) = \mu_{\text{I}}(x_i) + k_{\text{B}}T \ln\left(\frac{\overline{C}(x_i)}{1-\overline{C}(x_i)}\right), \tag{4}$$

where μ_{I} is their enthalpy while $\overline{C}(x_i) \equiv C_{\text{I}}(x_i)/C_{\text{r}}$ in terms of the number of integrin sites per unit area C_{r} on the cell membrane. The enthalpy of the integrins follows from recalling that each integrin molecule transmits a force $\mathcal{F}(x_i)$ related to the traction $\text{T}(x_i) \equiv \sqrt{\text{T}_1(x_i)^2 + \text{T}_2(x_i)^2}$ on the cell surface via $\text{T}(x_i) = \mathcal{F}(x_i)N_{\text{H}}$. Then,

$$\mu_{\text{I}}(x_i) = \Phi(\Delta(x_i)) - \mathcal{F}(x_i)\Delta(x_i), \tag{5}$$

where Δ is the stretch of the FA complex, and Φ the internal energy of the complex subjected to a stretch Δ. Now, assuming linear behavior of the complex with a stiffness κ_{s} such that $\mathcal{F}(x_i) \equiv \kappa_{\text{s}}\,\Delta(x_i)$, Eq. 5 reduces to $\mu_{\text{I}}(x_i) = -\mathcal{F}(x_i)^2/2\kappa_{\text{s}}$, and the chemical potential follows as such:

$$\chi_{\text{I}}(x_i) = k_{\text{B}}T \ln\left(\frac{\overline{C}(x_i)}{1-\overline{C}(x_i)}\right) - \frac{\mathcal{F}(x_i)^2}{2\kappa_{\text{s}}}. \tag{6}$$

The integrins are mobile over the surface membrane, and at equilibrium, their chemical potentials are spatially uniform such that $\chi_{\text{I}}(x_i) = \chi_{\text{C}}$. The equilibrium concentrations $\overline{C}_{\text{eq}}(x_i)$ then follow in terms of χ_{C} as follows:

$$\left(\frac{\overline{C}_{\text{eq}}(x_i)}{1-\overline{C}_{\text{eq}}(x_i)}\right) = \exp\left(\frac{\chi_{\text{C}} + \dfrac{\mathcal{F}(x_i)^2}{2\kappa_{\text{s}}}}{k_{\text{B}}T}\right). \tag{7}$$

However, χ_{C} is as yet unknown, and the conservation of integrins provides the additional constraint to determine χ_{C}, viz given a spatially uniform surface density C_0 of integrins for a cell in suspension, the conservation statement reads as follows:

$$A_0C_0 = C_{\text{r}} \int_A \overline{C}_{\text{eq}}(x_i)dA, \tag{8}$$

where A_0 is the surface area of the cell in suspension, and A is its area in the current configuration. The simultaneous solution of Eqs. 7 and 8 gives χ_{C}, and the adhesion free energy of the cell is then given as $F_{\text{adh}} = A_0C_0\chi_{\text{C}}$.

The above analysis assumes the adhesion complexes can sustain any required force $\mathcal{F}(x_i)$ via the assumed linearity of the complex response. However, it has been demonstrated that complexes cannot support a force greater than a critical value $\mathcal{F}_{\text{max}}$ (21–23). Direct enforcement of the condition that no complex force exceeds $\mathcal{F}_{\text{max}}$ at the cell-substrate interface would require an iterative adjustment of spread state (as implemented for simplified microstates by McEvoy et al. (13)) and is therefore excessively computationally expensive in the context of the Monte Carlo simulations required for sampling the homeostatic ensemble. Here, we use the alternative approach of a penalty scheme to ensure that a very small number of spread states contain complexes with forces $\mathcal{F} > \mathcal{F}_{\text{max}}$. In summary, we define a penalty force as follows:

$$\mathcal{F}^{\text{p}} = \int_A \Delta\mathcal{F}^{\text{p}}(x_i)\,dA, \tag{9}$$

where

$$\Delta\mathcal{F}^{\text{p}}(x_i) = \begin{cases} \mathcal{F}(x_i) - \mathcal{F}_{\text{max}} & \mathcal{F}(x_i) > \mathcal{F}_{\text{max}} \\ 0 & \text{otherwise.} \end{cases} \tag{10}$$

A penalty energy is then defined as $\chi_{\text{p}} = (\mathcal{F}^{\text{p}})^2/(2\kappa_{\text{p}})$, where the parameter κ_{p} has the units of stiffness and sets the magnitude of the penalty. The total FA free energy, including the penalty contribution, is then defined as follows:

$$F_{\text{adh}} = A_0C_0\left(\chi_{\text{C}} + \chi_{\text{p}}\right), \tag{11}$$

with the normalized energy $\widehat{F}_{\text{adh}}$ following from the definitions detailed in Supporting Materials and Methods (Section S2.4) along with the model parameters. To compare model predictions with the experimental results of Engler et al. (3), the number of ligands per unit area, N_{H}, can be expressed as surface collagen density ρ_{col} through the following expression:

$$\rho_{\text{col}} = N_{\text{H}}M_{\text{col}}/L\ , \tag{12}$$

where M_{col} is the molar mass of collagen, and L is Avogadro's constant. We assume a uniform surface collagen distribution and substrate stiffness.

RESULTS AND DISCUSSION

Spread dependence of cells on surface collagen density

The influence of surface collagen density ρ_{col} on cell spreading is shown in Fig. 1. Cells are spread on rigid substrates coated with three different values of ρ_{col} (6, 33, and 250 ng cm^{-2}). A sample of cell spread states, with the same free energy for a given ρ_{col}, are shown in Fig. 1 *a*, including SF distributions (*green*), FA distributions (*red*), and nuclei (*blue*). In the case of a low ρ_{col} (i.e., 6 ng cm^{-2}), cells are not highly spread, and they maintain regular rounded

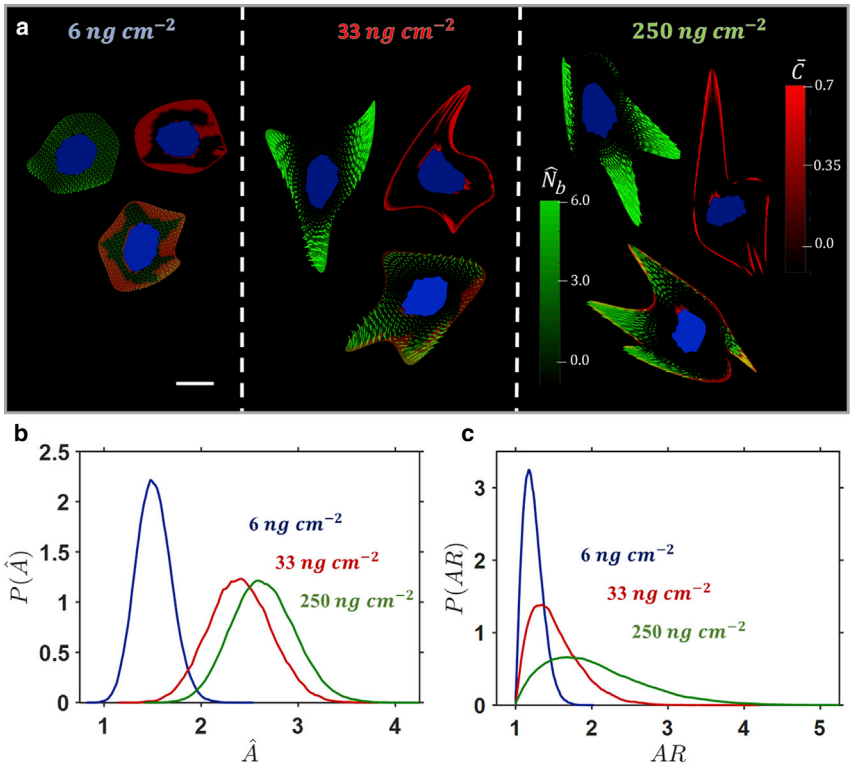

FIGURE 1 (*a*) Contours of bound SF protein concentrations $\widehat{N}_b$ (*green*) with dominant alignment, FA distributions $\widehat{C}$ (*red*), and overlays in commonly observed cell shapes at a given surface collagen density ρ_{col}. The substrate is rigid, and the nucleus is highlighted in blue. The cell spread states for a given ρ_{col} have the same free energy. The scale bar represents the undeformed cell radius R_0. Probability density functions (pdfs) for cells spread on a rigid substrate for three collagen densities of (*b*) cell spread area ($\widehat{A} = A/\pi R_0^2$) and (*c*) cell AR are shown. To see this figure in color, go online.

morphologies. A low-concentration smeared actin cytoskeleton is observed throughout the cell, with no regions of highly aligned SFs. For a higher ρ_{col} of 33 ng cm^{-2}, cells become more highly spread. Additionally, the spread shapes become quite irregular in contrast to the rounded shapes observed on a lower ρ_{col}. Regions of aligned SFs are observed, and FAs cluster toward the cell periphery. In the case of the highest ρ_{col} of 250 ng cm^{-2}, a further increase in spread area is observed, and the spread shape becomes highly irregular, with cells exhibiting elongated protrusions. High concentrations of aligned SFs are observed, and FAs are highly localized at the cell periphery and cell nucleus.

Probability density functions (pdfs) for cell spread area (Fig. 1 *b*) and for cell aspect ratio (AR) of a best-fit ellipse (Fig. 1 *c*) are constructed from the full population of spread states for each surface collagen density. With increasing ρ_{col}, the mean cell spread area increases, and the variance in spread area increases (i.e., in Fig. 1 *a*, as ρ_{col} increases, the pdf moves to the right and becomes less peaked). A similar trend is observed for cell AR (Fig. 1 *c*), for which the mean is closer to 1, and the variance is very low (the pdf is more peaked) for the lowest ρ_{col}. In summary, the pdfs presented in Fig. 1, *b* and *c* show that a population of cells on a lower ρ_{col} will have a lower mean spread area and a lower variance of spread area in addition to being rounded (AR close to 1) with a low variance of spread shape. As ρ_{col} increases, a higher mean spread area is obtained for a population of cells, with a higher variance of spread area and spread shape. Additional spread shapes are presented in Figs. S1 and S2.

Influence of substrate stiffness on cell spreading

The influence of substrate stiffness E_{sub} on cell spreading is shown in Fig. 2. Cells are spread on substrates of stiffness 8 and 32 kPa, in addition to a rigid substrate. All substrates have a ρ_{col} of 33 ng cm^{-2}. A sample of cell spread states shown in Fig. 2 *a* suggests that cell spread area increases with E_{sub}. Cells on the compliant (8 kPa) substrate exhibit a low-concentration smeared actin cytoskeleton, compared to the highly aligned SFs on the stiff and rigid substrate. The irregularity of the spread shape increases with E_{sub}, with longest protrusions occurring on the rigid substrate.

Pdfs for cell spread area (Fig. 2 *b*) and AR (Fig. 2 *c*) are constructed from the full population of spread states for each value of E_{sub}. Clearly, both the mean spread area and the variance in spread area increase with E_{sub} (i.e., in Fig. 2 *b*, the pdf moves to the right and becomes less peaked as E_{sub} is increased). The effect of E_{sub} on cell shape is less pronounced for the value of ρ_{col} considered here, with only a minor increase in the mean and variance of cell AR with increasing stiffness (Fig. 2 *c*).

Coupled dependence of collagen density and substrate stiffness

The coupled interplay between the influence of ρ_{col} and E_{sub} on cell spreading is next considered. Contour plots are constructed from mean spread areas (Fig. 3 *a*) and mean ARs (Fig. 3 *b*). Representative spread states are superimposed

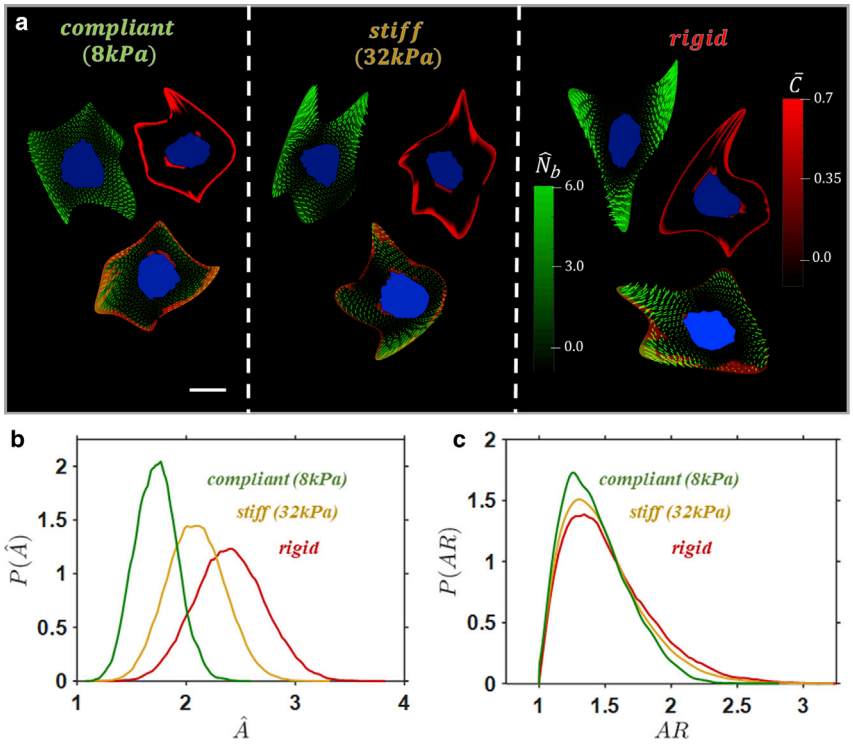

FIGURE 2 (*a*) Contours of bound SF protein concentrations $\widehat{N}_b$ (*green*) with dominant alignment, FA distributions $\widehat{C}$ (*red*), and overlays in commonly observed cell shapes at a given substrate stiffness E_{sub}. The surface collagen density ρ_{col} is fixed at 33 ng cm^{-2}, and the nucleus is highlighted in blue. The cell spread states for a given E_{sub} have the same free energy. The scale bar represents undeformed cell radius R_0. Probability density functions (pdfs) for cells spread on substrates of different stiffness at a surface collagen density ρ_{col} of 33 ng cm^{-2}, of (*b*) cell spread area ($\widehat{A} = A/\pi R_0^2$), and (*c*) cell AR are shown. To see this figure in color, go online.

for illustrative purposes. As shown in Fig. 3 *a*, a very low ρ_{col} results in a very weak dependence of mean spread area on E_{sub}. However, for moderate and high ρ_{col}, the mean spread area is highly dependent on E_{sub}. As shown in Fig. 3 *b*, the cell AR exhibits a very weak dependence on E_{sub} (the contours in Fig. 4 *b* are almost uniform in the vertical direction), while exhibiting a very strong dependence on ρ_{col}.

Both the mean and SD of cell spread area is shown in Fig. 3 *c*. A number of features should be noted: 1) as ρ_{col} is increased, both the mean and SD increase up to a peak value (this trend is observed for all values of E_{sub}); 2) if ρ_{col} is increased beyond the peak value, a slight reduction in mean spread area (and its SD) is observed; again, this trend is observed for all values of E_{sub}; 3) the ρ_{col} at which the mean spread area reaches a peak value increases with increasing E_{sub}; and 4) for a given ρ_{col}, both the mean and SD increase with increasing E_{sub}. Fig. 3 *d* shows that cell AR is highly dependent on ρ_{col}, with both the mean and SD increasing with increasing ρ_{col}. It is interesting to note that even though the cell mean spread area decreases when the ρ_{col} is increased beyond the critical value, the mean AR continues to increase. However, the mean AR and its SD exhibit a weak dependence on E_{sub}.

Experimental support for predicted cell behavior

Remarkably, all the features described by Fig. 3 are directly supported by the experimental study of Engler et al. (3) in which the response of SMCs to E_{sub} and ρ_{col} was investigated. At a low ρ_{col} on all substrates, SMCs that were detectably spread were found to be rounded with a low spread area. As the ρ_{col} was increased, the spread area (mean and SD) was observed to increase up to a peak value. After this peak, any increase to the density of ρ_{col} resulted in a reduction of mean spread area. This behavior is further supported by the experimental study of Gaudet et al. (24). Engler et al. (3) noted that the ρ_{col} at which the peak mean spread area occurs is dependent on E_{sub}, that is, it increases with increasing E_{sub}, as predicted by our models). They also reported that an increase in E_{sub} results in a higher mean cell spread area for a fixed ρ_{col}.

Although the AR is not directly measured in the experimental work of Engler et al. (3), with an increase in cell area (because of E_{sub} or ρ_{col}), it was reported that cell shapes became less rounded and more irregular when cell spread area increases as a result of increased E_{sub} and/or ρ_{col}. Such a reduction in cell roundness with increasing E_{sub} has also been observed in the experimental study of Ren et al. (25) for skeletal muscle cells. Additionally, Prager-Khoutorsky et al. (26) reported that cells readily elongate (i.e., high AR) when plated on rigid substrates, with the behavior significantly less pronounced with decreasing E_{sub}. Similar to our predictions for SF distributions, Engler et al. (3) report that highly spread cells display a well-ordered SF network. Such ordered fibers were far less probable on rounded cells on low ρ_{col} and on softer substrates. Similar observations are also reported in the experimental study by Deroanne et al. (27) in which a significant reduction in SF and FAs formation was observed in endothelial

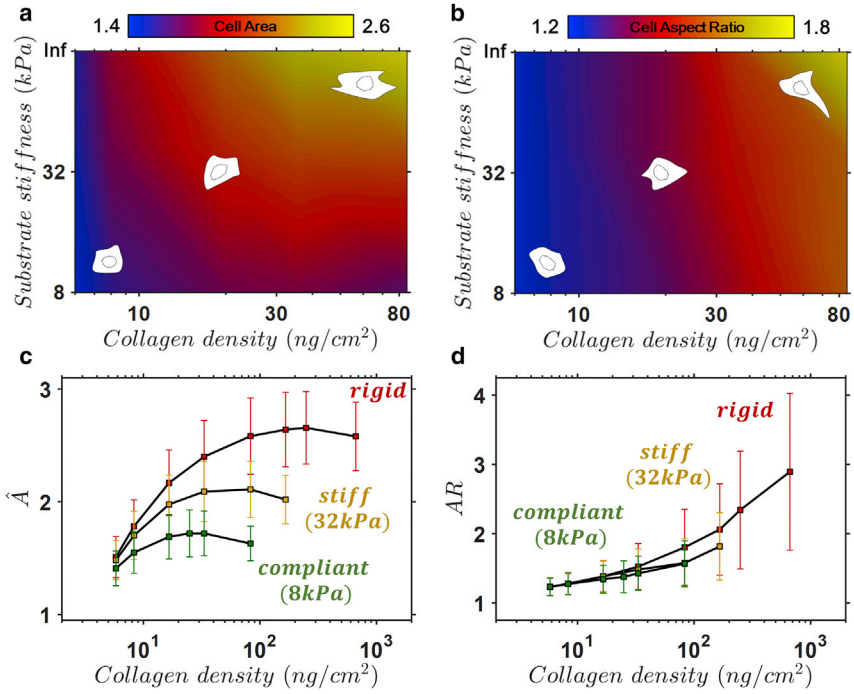

FIGURE 3 Contour plots for predicted mean spread area (*a*) and mean cell AR (*b*) in the $\rho_{col} - E_{sub}$ space. (*c*) The predicted cell area (mean ± SD) and (*d*) cell AR (mean ± SD) as a function of surface collagen density ρ_{col} for cells spread on substrates of different stiffness (*red*: rigid; *yellow*: 32 kPa; *green*: 8 kPa). Sample cell spread states are shown for a given substrate in (*a* and *b*). To see this figure in color, go online.

cells on soft gels compared to stiff substrates. Pelham and Wang (28) also showed such dependence of adhesion formation on substrate stiffness. The predicted trends of SF and FA organization in Figs. 1 and 2 of the current study are strongly supported by the aforementioned experimental studies. Additional samples of computed cell spread states are shown in Figs. S1 and S2.

Thermodynamically motivated insights and explanations for predicted cell behavior

We next provide a thermodynamically motivated explanation for the computed results in Figs. 1 and 3 and, by extension, for the experimental observations of Engler et al. (3). In Fig. 4 *a*, we plot the pdf of Gibbs free energy for the three values of ρ_{col} on a rigid substrate. Recall that the system is subject to the homeostatic constraint such that the mean Gibbs free energy of all states is equal to the cellular homeostatic free energy G_S, which can be identified from the unique state of a freestanding cell. Therefore, the mean free energy is similar for all values of ρ_{col} (Fig. 4 *a*). The pdf for adhesion free energy (Fig. 4 *b*) is highly peaked and negative for a high ρ_{col} of 250 ng cm^{-2}. This indicates a high probability that adhesion complex forces are close to $\mathcal{F}_{max}$ so that a low adhesion energy is obtained. On the other hand, there is a low probability that adhesion complex forces exceed $\mathcal{F}_{max}$ and incur a positive adhesion energy penalty.

In the case of a high ρ_{col} of 250 ng cm^{-2}, the cell-substrate tractions for a wide range of highly spread states can be supported without incurring an adhesion energy penalty (i.e., the adhesion free energy remains low). As a result, the entropy of spread states is very high for high values of ρ_{col}. Correspondingly, a high variance in the (negative) cytoskeletal and (positive) elastic free energies (Fig. 4, *c* and *d*) occurs. In effect, cell spreading on a rigid substrate coated with a high ρ_{col} can be viewed as a competition between positive elastic free energy due to stretching of passive cell components and negative free energy due to the assembly of contractile SFs, with an additional negative free-energy contribution from the adhesion complexes.

When ρ_{col} is reduced, higher forces occur in ligand complexes, resulting in a higher probability that $\mathcal{F}_{max}$ is exceeded and an adhesion energy penalty is incurred. Therefore, there is a low probability that highly spread states will occur, and the entropy of spread states decreases. In other words, a highly spread cell on a low ρ_{col} will result in adhesion complex forces that exceed the maximal value, and the imposition of an energetic penalty results in a low probability that such highly spread states will occur. This explains the high probability of rounded cells with low spread areas on a ρ_{col} of 6 ng cm^{-2}, as reported in Figs. 1 and 3. Correspondingly, as shown in Fig. 4, *c* and *d*, the cytoskeletal and elastic free-energy pdfs are highly peaked with mean values close to zero (as expected for the observed low spread areas and low variance in spread shapes (AR)).

Recall from Fig. 3 that for all values of E_{sub}, cell spread area increases with increasing ρ_{col} up to a peak value. In Fig. 5, we report the mean and SD of the free-energy densities across all ρ_{col} and E_{sub} (the SD is indicative of the

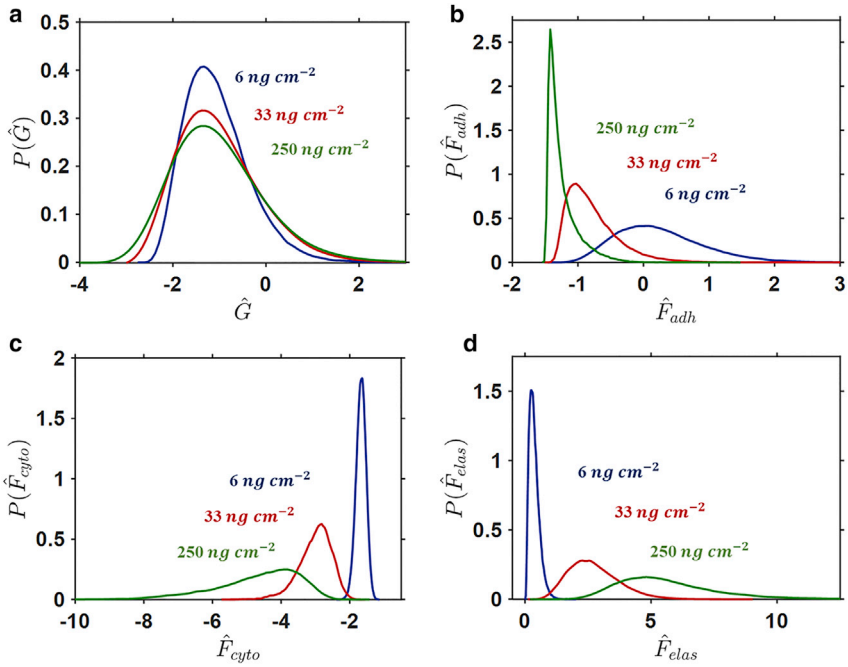

FIGURE 4 Probability density functions (pdfs) for cells spread on a rigid substrate for three surface collagen densities ρ_{col} of (*a*) Gibbs free energy, (*b*) adhesion free energy, (*c*) cytoskeletal free energy, and (*d*) elastic free energy ($\widehat{F}_{elas} = \widehat{F}_{passive} + \widehat{F}_{sub}$). To see this figure in color, go online.

variance observed in the corresponding pdfs). The peak spread areas shown in Fig. 3 *b* coincide with the lowest mean adhesion free energy for each substrate (Fig. 5, *a–c*). The ρ_{col} associated with such a peak spread area on each substrate is hereafter referred to as "optimal." At this optimal ρ_{col}, there is a high probability that the forces in adhesion complexes will result in a low adhesion free energy. For suboptimal ρ_{col}, highly spread states will result in an increased probability of adhesion complex forces higher than $\mathcal{F}_{max}$, resulting in an energetic penalty, as explained in Fig. 4 above. On the other hand, when the ρ_{col} is increased beyond the "optimal" value, the cell must spread to a higher area to generate sufficient tractions to achieve sufficiently high adhesion complex forces (i.e., $\mathcal{F}(x_i) \cong \mathcal{F}_{max}$) and a low adhesion free energy. However, spreading to such a high area results in an increased elastic strain energy. There is a low probability that the adhesion (Fig. 5, *a–c*) and cytoskeletal (Fig. 5, *d–f*) free energy will overcome this "elastic penalty" and achieve the homeostatic state (i.e., $\widehat{G}_S$). Therefore, on "postoptimal" ρ_{col}, there is a low probability that the cell area will increase beyond the peak spread area. In fact, a postoptimal ρ_{col} leads to a reduction in mean spread area, as shown in Fig. 3 *c* (this has been also observed experimentally by Engler et al. (3) and Gaudet et al. (24), discussed in Experimental Support for Predicted Cell Behavior above). This occurs because cellular tractions are supported by a higher number of complexes so that individual bond forces are reduced. Therefore, the cell adhesion free energy moves toward zero (Fig. 5, *a–c*), providing a weaker competition to the elastic strain energy (Fig. 5, *g–i*) so that there is a lower probability that the cell will achieve the peak spread area. Although the mean spread area decreases for postoptimal ρ_{col}, the mean elastic free energy increases on rigid and stiff substrates (Fig. 5, *g* and *h*). This is because of a high variability in spread shape on stiffer substrates with high ρ_{col} (see plots of cell AR in Fig. 3 *d*).

A reduction in E_{sub} lowers the probability of the cell achieving a high spread area, with rounded low-spread morphologies more frequently observed (Fig. 3 *c*). On a rigid substrate, there is no contribution from the elastic strain energy of the substrate (Fig. 5 *j*) because it is not deformed by the contractile activity of the cell. However, as the E_{sub} is reduced (Fig. 5, *k* and *l*), it will be deformed by the cell. The associated substrate free energy causes the total system free energy to become increasingly positive. Thus, to achieve a homeostatic state, there is a high probability that the cell area will be lower on more compliant substrates. The highly coupled balance between the contributions to the system free energy causes the peak cell area to occur at a lower ρ_{col} for a lower E_{sub}. As mentioned above, a low E_{sub} results in lower spread areas, which leads to lower cell-substrate tractions. Therefore, a lower ρ_{col} is required for an increased probability of optimal forces in adhesion complexes ($\mathcal{F}(x_i) \cong \mathcal{F}_{max}$) and a correspondingly low adhesion free energy. Peak spreading occurs on lower ρ_{col} for lower E_{sub}, as shown in Fig. 3 *c* (and as reported in the experiments of Engler et al. (3)).

CONCLUSIONS

The equilibrium statistical mechanics framework developed by Shishvan et al. (15) allows for the simulation of the homeostatic ensemble for cells on an elastic substrate

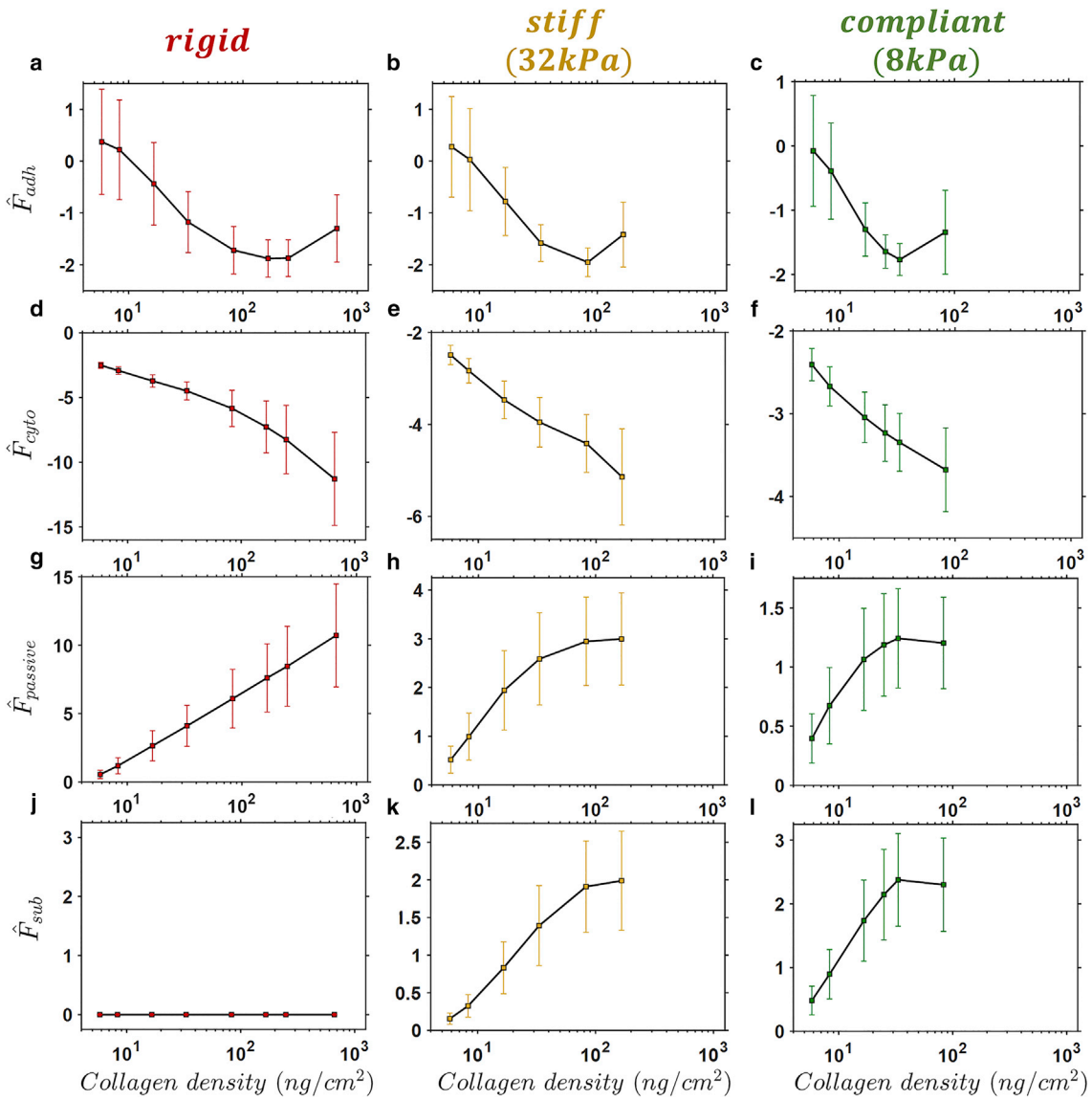

FIGURE 5 Predicted adhesion (*a–c*), cytoskeletal (*d–f*), elastic (*g–i*), and substrate (*j–l*) free energy (mean ± SD) as a function of surface collagen density ρ_{col} for cells spread on rigid, stiff, and compliant substrates. To see this figure in color, go online.

in a nutrient bath. Cells assume a dynamic homeostatic equilibrium by means of a free-energy competition between the increasing elastic free energy due to stretching of passive cell components (and substrate deformation) and the decreasing cytoskeletal free energy as contractile proteins assemble to form SFs. In the current study, the framework is expanded to include the free energy associated with the formation of FAs between the cell and a collagen-coated substrate.

The expanded framework allows for the simulation of the coupled influence of surface collagen density ρ_{col} and substrate stiffness E_{sub} on cell spreading, as reported in the experimental study of Engler et al. (3). The key experimental observations predicted by our modeling framework are summarized as follows:

1) With increasing substrate ρ_{col}, cell spread area (mean and SD) increases up to a peak value.
2) A further increase in ρ_{col} beyond this peak results in a reduction of the cell spread area (mean and SD).
3) The ρ_{col} at which the mean cell area reaches a peak decreases with decreasing E_{sub}.
4) At a fixed ρ_{col}, the mean and SD of the spread area increase with increasing E_{sub}.

The ρ_{col} directly influences the forces in adhesion complexes and, consequently, the adhesion free energy. This, in turn, influences the spread states that cells assume in achieving homeostasis. A low ρ_{col} lowers the probability of a cell becoming highly spread, because sufficient complexes cannot form to support the tractions imposed

by the substrate. Conversely, at a high ρ_{col}, the cell may form more adhesion complexes, lowering the associated free energy. Thus, the probability of cells having a high spread area increases. The influence of E_{sub} and ρ_{col} is highly coupled, as demonstrated in Figs. 3 and 5. A deformable substrate lowers the probability of a cell becoming highly spread, reducing the cell tractions and thereby causing the peak mean spread area to occur at a lower ρ_{col}.

In statistical thermodynamics, a closed system in a constant temperature and pressure environment attains equilibrium at minimal Gibbs free energy. However, metabolic systems such as cells cannot be viewed in this manner; in fact, cells never attain an equilibrium minimal free-energy state while alive. The approach developed by Shishvan et al. (15) (extended in the current study) acknowledges this and predicts the statistics of biological observables (e.g., cell area, AR, etc.) under the constraint that the cell maintains a homeostatic state. In previous studies, the importance of considering the system free energy in the interpretation of cell-spreading behavior has been recognized (13,29). McEvoy et al. (13) identified low (or minimal) free-energy cell spread states within a limited phase space of axisymmetric configurations. This simplified approach provided a reasonable approximation of the detailed trends computed in the current study (as observed experimentally (3)), which can be explained by the fact that low free-energy states will of course be highly probable within the homeostatic ensemble; see Eq. 1. Although McEvoy et al. (13) correctly demonstrate that cell spreading is governed by a competition between decreasing cytoskeletal and adhesion free energy and increasing elastic energy, the identification of a low or minimal free-energy configuration is not physically appropriate for a fluctuating system. Therefore, the emergence of such an energetic competition within the statistical mechanics framework of the homeostatic ensemble provides a significant advance in current understanding of the influence of ligand density and substrate stiffness on cell spreading. Importantly, this framework correctly predicts the trends for observables such as the spread area and spread shape as a function of environmental cues, such as stiffness and ligand density, and quantifies inherent statistical variability in these observations. The homeostatic ensemble for cells, expanded to include the FA formation and an associated adhesion free-energy contribution, provides new insight into observed cell behavior on deformable collagen-coated substrates. The model may readily be used to simulate more complex extracellular environments, including the spreading of cells on ligand patterned ridges and ligand patterned micropillars. Furthermore, the computational framework will be extended in a future study to explore the influence of gradients of ligand density on cell motility.

SUPPORTING MATERIAL

Supporting Materials and Methods and four figures are available at http://www.biophysj.org/biophysj/supplemental/S0006-3495(18)31228-1.

AUTHOR CONTRIBUTIONS

All authors contributed to the development and implementation of the computational model. E.M. performed all simulations and created all figures. E.M., J.P.M., and V.S.D. analyzed the results and wrote the article. J.P.M. and V.S.D. designed and coordinated the research.

ACKNOWLEDGMENTS

Grant support was provided by the Irish Research Council postgraduate scholarship (GOIPG/2015/2954), the National University of Ireland Galway Hardiman scholarship, and the Science Foundation Ireland (SFI-12/IP/1723). The authors acknowledge the Irish Centre for High-End Computing for the provision of computational facilities and support.

REFERENCES

1. Lange, L. A., D. W. Bowden, …, B. I. Freedman. 2002. Heritability of carotid artery intima-medial thickness in type 2 diabetes. *Stroke.* 33:1876–1881.
2. Chow, M. J., R. Turcotte, …, Y. Zhang. 2014. Arterial extracellular matrix: a mechanobiological study of the contributions and interactions of elastin and collagen. *Biophys. J.* 106:2684–2692.
3. Engler, A., M. Sheehan, …, D. E. Discher. 2003. Substrate compliance vs ligand density in cell on gel responses. *Eur. Cell. Mater.* 6:7–8.
4. Jacot, J. G., A. D. McCulloch, and J. H. Omens. 2008. Substrate stiffness affects the functional maturation of neonatal rat ventricular myocytes. *Biophys. J.* 95:3479–3487.
5. Arnold, M., E. A. Cavalcanti-Adam, …, J. P. Spatz. 2004. Activation of integrin function by nanopatterned adhesive interfaces. *Chemphyschem.* 5:383–388.
6. Ronan, W., V. S. Deshpande, …, J. P. McGarry. 2014. Cellular contractility and substrate elasticity: a numerical investigation of the actin cytoskeleton and cell adhesion. *Biomech. Model. Mechanobiol.* 13:417–435.
7. McGarry, J. P., J. Fu, …, V. S. Deshpande. 2009. Simulation of the contractile response of cells on an array of micro-posts. *Philos Trans A Math Phys Eng Sci.* 367:3477–3497.
8. Pirentis, A. P., E. Peruski, …, D. Stamenović. 2011. A model for stress fiber realignment caused by cytoskeletal fluidization during cyclic stretching. *Cell. Mol. Bioeng.* 4:67–80.
9. Vernerey, F. J., and M. Farsad. 2014. A mathematical model of the coupled mechanisms of cell adhesion, contraction and spreading. *J. Math. Biol.* 68:989–1022.
10. Vernerey, F. J., and U. Akalp. 2016. Role of catch bonds in actomyosin mechanics and cell mechanosensitivity. *Phys. Rev. E.* 94:012403.
11. Mogilner, A., and B. Rubinstein. 2005. The physics of filopodial protrusion. *Biophys. J.* 89:782–795.
12. Akalp, U., C. Schnatwinkel, …, F. J. Vernerey. 2017. Structural modeling of mechanosensitivity in non-muscle cells: multiscale approach to understand cell sensing. *ACS Biomater. Sci. Eng.* 3:2934–2942.
13. McEvoy, E., V. S. Deshpande, and P. McGarry. 2017. Free energy analysis of cell spreading. *J. Mech. Behav. Biomed. Mater.* 74:283–295.
14. Théry, M., A. Pépin, …, M. Bornens. 2006. Cell distribution of stress fibres in response to the geometry of the adhesive environment. *Cell Motil. Cytoskeleton.* 63:341–355.

15. Shishvan, S. S., A. Vigliotti, and V. S. Deshpande. 2018. The homeostatic ensemble for cells. *Biomech. Model. Mechanobiol.* 17:1631–1662.

16. Jaynes, E. T. 1957. Information theory and statistical mechanics. *Phys. Rev.* 106:620–630.

17. Vigliotti, A., W. Ronan, …, V. S. Deshpande. 2016. A thermodynamically motivated model for stress-fiber reorganization. *Biomech. Model. Mechanobiol.* 15:761–789.

18. Weafer, P. P., W. Ronan, …, J. P. McGarry. 2013. Experimental and computational investigation of the role of stress fiber contractility in the resistance of osteoblasts to compression. *Bull. Math. Biol.* 75:1284–1303.

19. Reynolds, N. H., W. Ronan, …, J. P. McGarry. 2014. On the role of the actin cytoskeleton and nucleus in the biomechanical response of spread cells. *Biomaterials.* 35:4015–4025.

20. Dowling, E. P., W. Ronan, …, J. P. McGarry. 2012. The effect of remodelling and contractility of the actin cytoskeleton on the shear resistance of single cells: a computational and experimental investigation. *J. R. Soc. Interface.* 9:3469–3479.

21. Dowling, E. P., and J. P. McGarry. 2014. Influence of spreading and contractility on cell detachment. *Ann. Biomed. Eng.* 42:1037–1048.

22. McGarry, J. P., and P. E. McHugh. 2008. Modelling of in vitro chondrocyte detachment. *J. Mech. Phys. Solids.* 56:1554–1565.

23. Selhuber-Unkel, C., T. Erdmann, …, J. P. Spatz. 2010. Cell adhesion strength is controlled by intermolecular spacing of adhesion receptors. *Biophys. J.* 98:543–551.

24. Gaudet, C., W. A. Marganski, …, J. Y. Wong. 2003. Influence of type I collagen surface density on fibroblast spreading, motility, and contractility. *Biophys. J.* 85:3329–3335.

25. Ren, K., L. Fourel, …, C. Picart. 2010. Manipulation of the adhesive behaviour of skeletal muscle cells on soft and stiff polyelectrolyte multilayers. *Acta Biomater.* 6:4238–4248.

26. Prager-Khoutorsky, M., A. Lichtenstein, …, A. D. Bershadsky. 2011. Fibroblast polarization is a matrix-rigidity-dependent process controlled by focal adhesion mechanosensing. *Nat. Cell Biol.* 13:1457–1465.

27. Deroanne, C. F., C. M. Lapiere, and B. V. Nusgens. 2001. In vitro tubulogenesis of endothelial cells by relaxation of the coupling extracellular matrix-cytoskeleton. *Cardiovasc. Res.* 49:647–658.

28. Pelham, R. J., Jr., and -gnskip-->Yl. Wang. 1997. Cell locomotion and focal adhesions are regulated by substrate flexibility. *Proc. Natl. Acad. Sci. USA.* 94:13661–13665.

29. Shenoy, V. B., H. Wang, and X. Wang. 2016. A chemo-mechanical free-energy-based approach to model durotaxis and extracellular stiffness-dependent contraction and polarization of cells. *Interface Focus.* 6:20150067.

Biophysical Journal, Volume *115*

Supplemental Information

Thermodynamic Modeling of the Statistics of Cell Spreading on Ligand-Coated Elastic Substrates

Eoin McEvoy, Siamak S. Shishvan, Vikram S. Deshpande, and J. Patrick McGarry

SUPPLEMENTARY INFORMATION

1. The homeostatic statistical mechanics framework

Here, we provide a brief overview of the homeostatic mechanics framework of Shishvan *et al.* (1) with the aim to provide the reader the key aspects of the framework required for fully appreciating the computational results presented in the main text. Readers are referred to Shishvan *et al.* (1) for a more complete treatment including the derivations of the relevant equations.

Making the ansatz that *living cells are entropic*, Shishvan *et al*. (1) introduced the concept of the *homeostatic ensemble* with cellular homeostasis providing the additional constraints and mechanisms for entropy maximisation. This defined the notion of a (dynamic) *homeostatic equilibrium* state that intervenes to allow living cells to elude thermodynamic equilibrium. They thus developed a statistical mechanics framework for living cells using the notions of statistical inference (2) applicable over a timescale from a few hours to a few days as long as the cell remains as a single undivided entity (i.e. the interphase period of the cell cycle). The key ideas behind the framework can be summarised as follows. A system comprising the cell and the extracellular matrix (ECM) is an open system with the cell exchanging nutrients with the surrounding bath. These nutrients fuel a large number of coupled biochemical reactions that include actin polymerisation, treadmilling and dendritic nucleation that effect changes to the cell morphology. These biochemical reactions change the morphology of the cell but are not precisely controlled, and this manifests via the observed morphological fluctuations of the cell. Shishvan *et al*. (1) made the *ansatz* that these biochemical reactions provide the mechanisms to maximise the morphological entropy of the cell, but constrained by the fact that the cell maintains a homeostatic state over the interphase period. Cellular homeostasis is the ability of cells to actively regulate their internal state, and maintain the concentration of all internal species[1] at specific average values over their morphological fluctuations independent of the environment.

[1] Chemical species here are defined in a manner analogous to the Gibbs definition for a grand canonical ensemble, viz. chemical species are an ensemble of chemically identical molecular entities that can explore the same set of molecular energy levels on the timescale of a morphological microstate.

1.1. Morphological microstates, entropy, fluctuations, and the homeostatic temperature

Controlling only macro variables (i.e. macrostate) such as the temperature, pressure, and nutrient concentrations in the nutrient bath results in inherent uncertainty (referred to here as missing information) in micro variables (i.e. microstates) of the system. This includes a level of unpredictability in homeostatic process variables, such as the spatio-temporal distribution of chemical species, that is linked to Brownian motion and the complex feedback loops in the homeostatic processes. Thus, this system not only includes the usual lack of precise information on the positions and velocities of individual molecules associated with the thermodynamic temperature, but also an uncertainty in cell shape resulting from imprecise regulation of the homeostatic processes. The consequent entropy production forms the basis of this new statistical mechanics framework motivated by the following two levels of microstates:

(i) *Molecular microstates*. Each molecular microstate has a specific configuration (position and momentum) of all molecules within the system.

(ii) *Morphological microstates*. Each morphological microstate is specified by the mapping (connection) of material points on the cell membrane to material points on the collagen coated substrate. In broad terms, a morphological microstate specifies the shape and size of the cell.

Shishvan *et al*. (1) identified the (dynamic) homeostatic or equilibrium state of the system by entropy maximisation. Subsequently, we shall simply refer to this state as an equilibrium state to emphasise that it is a stationary macrostate of the system inferred via entropy maximisation as in conventional equilibrium analysis. The total entropy of the system is written in terms of the conditional probability $P^{(i|j)}$ of the molecular microstate (i) given the morphological microstate (j) and the probability $P^{(j)}$ of morphological microstate (j) as

$$I_{\mathrm{T}} = \sum_{j} P^{(j)} I_{\mathrm{M}}^{(j)} + I_{\Gamma}. \tag{S1}$$

In eq. (S1), $I_{\mathrm{M}}^{(j)} \equiv -\sum_{i\in j} P^{(i|j)} \ln P^{(i|j)}$ and $I_{\Gamma} \equiv -\sum_{j} P^{(j)} \ln P^{(j)}$ are the entropies of molecular microstates in morphological microstate (j) and the morphological microstates, respectively. Equilibrium then corresponds to molecular and morphological macrostates that maximise I_{T} subject to appropriate constraints. The molecular macrostate evolves on the order of seconds, limited by processes such as the diffusion of unbound actin. By contrast, transformation of the morphological macrostate involves cell shape changes and therefore,

the morphological macrostate evolves on the order of minutes, limited by co-operative cytoskeletal processes within the cell such as meshwork actin polymerisation and dendritic nucleation. The evolutions of the molecular and morphological macrostates are therefore temporally decoupled, and Shishvan *et al*. (1) showed that eq. (S1) can be maximised by independently maximising $I_{\mathrm{M}}^{(j)}$ at the smaller timescale to determine the equilibrium distribution of molecular microstates for a given morphological microstate, and then maximising I_{Γ} at the larger timescale to determine the equilibrium distribution of the morphological microstates.

Over the (short) timescale on the order of seconds, the only known constraint on the system is that it is maintained at a constant temperature, pressure and strain distribution. The equilibrium of a given morphological microstate (j) obtained by maximising $I_{\mathrm{M}}^{(j)}$ (denoted by $S_{\mathrm{M}}^{(j)}$) corresponds to molecular arrangements that minimise the Gibbs free-energy with $G^{(j)}$. Since the connection between the cell and the collagen coated substrate is fixed for a given morphological microstate, the determination of $G^{(j)}$ is a standard boundary value problem as described in Section 2.2. Over the (long) timescale on the order of several minutes to hours, the equilibrium distribution $P_{\mathrm{eq}}^{(j)}$ is determined by maximising I_{Γ}, but now with the additional constraint that the cell is maintained in its homeostatic state. For the case of a cell on an ECM in a constant temperature and pressure nutrient bath, the homeostatic constraint translates to the fact that the average Gibbs free-energy of the system over all the morphological microstates it assumes, is equal to the equilibrium Gibbs free-energy G_{S} of an isolated cell in suspension (free-standing cell), i.e. the homeostatic processes maintain the average biochemical state of the system equal to that of a cell in suspension. In deriving this result, Shishvan *et al*. (1) did not consider every individual homeostatic process, but rather used just the coarse-grained outcome of the homeostatic processes. The application of this coarse-grained constraint is the key element of the *homeostatic mechanics* framework, with the morphological entropy I_{Γ} parameterising the information lost by not modelling all variables associated with the homeostatic processes.

The maximisation of I_{Γ} while enforcing $\sum_j P^{(j)} G^{(j)} = G_{\mathrm{S}}$ gives the *homeostatic equilibrium* state such that

$$P_{\mathrm{eq}}^{(j)} = \frac{1}{Z} \exp\left(-\zeta G^{(j)}\right), \tag{S2}$$

where $Z \equiv \sum_j \exp\left(-\zeta G^{(j)}\right)$ is the partition function of the morphological microstates, and the distribution parameter ζ follows from the homeostatic constraint

$$\frac{1}{Z}\sum_j G^{(j)} \exp\left(-\zeta G^{(j)}\right) = G_{\mathrm{S}}\,. \tag{S3}$$

The collection of all possible morphological microstates that the system assumes while maintaining its homeostatic equilibrium state is referred to as the *homeostatic ensemble*. The homeostatic ensemble can therefore be viewed as a large collection of copies of the system, each in one of the equilibrium morphological microstates. The copies (j) are distributed in the ensemble such that the free-energies $G^{(j)}$ follow an exponential distribution $P_{\mathrm{eq}}^{(j)}$ with the distribution parameter ζ.

The equilibrium morphological entropy $S_\Gamma = -\sum_j P_{\mathrm{eq}}^{(j)} \ln P_{\mathrm{eq}}^{(j)}$ (i.e. the maximum value of I_Γ) follows from (S2) as

$$S_\Gamma = \zeta G_{\mathrm{S}} + \ln Z, \tag{S4}$$

where $P_{\mathrm{eq}}^{(j)}$ is substituted from eq. (S2). Thus, S_Γ is related to ζ via the conjugate relation $\partial S_\Gamma/\partial G_{\mathrm{S}} = \zeta$. Thus, analogous to $1/T$ that quantifies the increase in uncertainty of the molecular microstates (i.e. molecular entropy $S_{\mathrm{M}}^{(j)}$) with average enthalpy, ζ specifies the increase in uncertainty of the morphological microstates (i.e. morphological entropy S_Γ) with the average Gibbs free-energy. We therefore refer to $1/\zeta$ as the *homeostatic temperature* with the understanding that it quantifies the fluctuations on a timescale much slower than that characterised by T.

2. The equilibrium Gibbs free-energy of a morphological microstate

Similar to conventional statistical mechanics calculations that require a model for the energy of the system, the homeostatic statistical mechanics framework requires a model for the Gibbs free-energy $G^{(j)}$ of morphological microstate (j). Here, we calculate $G^{(j)}$ using the free-energy model of Vigliotti *et al*. (3) (as modified by Shishvan *et al*. (1)) that includes contributions from cell elasticity and the actin/myosin stress-fibre cytoskeleton, with the cell modelled as a two-dimensional (2D) body in the $x_1 - x_2$ plane adhered to a deformable collagen coated substrate, such that the out-of-plane Cauchy stress $\Sigma_{33} = 0$. The key differences are that (i) we include a nucleus that was neglected in Shishvan *et al*. (1) (ii) and also add in explicit contribution from the focal adhesions as described in the main body of the paper. The state of the system changes as the cell moves, spreads, and changes shape on the substrate. Here, we shall give a prescription to calculate the Gibbs free-energy of the system when the cell is in a specific morphological microstate (j), where the connections of material points on the cell membrane to the surface of the collagen coated substrate are specified.

With the system comprising the cell and substrate within a constant temperature and pressure nutrient bath, the equilibrium value of the Gibbs free-energy $G^{(j)}$ of the system in morphological microstate (j) is given by $G^{(j)} = F_{\text{cell}}^{(j)} + F_{\text{sub}}^{(j)} + F_{\text{adh}}^{(j)}$. Here $F_{\text{adh}}^{(j)}$ is the free-energy associated with the formation of focal adhesion as described in the main paper body (see Section 2.3 therein). Moreover, we assume the substrate to be linear elastic so $F_{\text{sub}}^{(j)}$ is calculated directly from knowing the tractions the cells exert on a linear elastic half-space. Thus, we focus our description on the calculation of the free-energy of the cell $F_{\text{cell}}^{(j)}$. In the following, for the sake of notational brevity, we shall drop the superscript (j) that denotes the morphological microstate, as the entire discussion refers to a single morphological microstate.

The Vigliotti *et al*. (3) model assumes only two elements within the cell: (i) a passive elastic contribution from elements such as the cell membrane, intermediate filaments and microtubules, and (ii) an active contribution from contractile acto-myosin stress-fibres that are modelled explicitly. This model was modified in Shishvan *et al.* (1) to incorporate a non-dilute concentration of stress-fibres and here we further modify this model by including the nucleus in the analysis as a passive elastic body, in addition to the cytoplasm comprising the two above mentioned components. We shall first describe the modelling of the active acto-

myosin stress-fibres in the cytoplasm and then discuss the elastic model of both the nucleus and the cytoplasm.

Consider a two-dimensional (2D) cell of thickness b_0 and volume V_0 in its elastic resting state comprising a nucleus of volume V_{N} and cytoplasm of volume V_{C} such that $V_0 = V_{\mathrm{N}} + V_{\mathrm{C}}$. The representative volume element (RVE) of the stress-fibres within the cytoplasm in this resting configuration is assumed to be a cylinder of volume $V_{\mathrm{R}} = \pi b_0 (n^{\mathrm{R}} \ell_0/2)^2$, where ℓ_0 is the length of a stress-fibre functional unit in its ground-state, and n^{R} is the number of these ground-state functional units within this reference RVE. The total number of functional unit packets within the cell is N_0^{T}, and we introduce $N_0 = N_0^{\mathrm{T}} V_{\mathrm{R}}/V_{\mathrm{C}}$ as the average number of functional unit packets available per RVE; N_0 shall serve as a useful normalisation parameter. The state of stress-fibres at location x_i within the cell is described by their angular concentration $\eta(x_i, \varphi)$, and there are $n(x_i, \varphi)$ functional units in series along the length of each stress-fibre in the RVE. Here, φ is the angle of the stress-fibre bundle in the undeformed configuration with respect to the $x_2 -$ direction. Vigliotti *et al.* (3) showed that, at steady-state, the number n^{ss} of functional units within the stress-fibres is given by

$$\hat{n}^{\mathrm{ss}} \equiv \frac{n^{\mathrm{ss}}}{n^{\mathrm{R}}} = \frac{[1 + \varepsilon_{\mathrm{nom}}(x_i, \varphi)]}{1 + \tilde{\varepsilon}_{\mathrm{nom}}^{\mathrm{ss}}}, \tag{S5}$$

where $\tilde{\varepsilon}_{\mathrm{nom}}^{\mathrm{ss}}$ is the strain at steady-state within a functional unit of the stress-fibres, and $\varepsilon_{\mathrm{nom}}(x_i, \varphi)$ is the nominal strain in direction φ. The chemical potential of the functional units within the stress-fibres in terms of the Boltzmann constant k_{B} is given by

$$\chi_{\mathrm{b}} = \frac{\mu_{\mathrm{b}}}{n^{\mathrm{R}}} + k_{\mathrm{B}} T \ln \left[\left(\frac{\pi \hat{\eta}\, \hat{n}^{\mathrm{ss}}}{\widehat{N}_{\mathrm{u}} \left(1 - \dfrac{\hat{\eta}}{\hat{\eta}_{\mathrm{max}}} \right)} \right)^{\frac{1}{n^{\mathrm{ss}}}} \left(\frac{\widehat{N}_{\mathrm{u}}}{\pi \widehat{N}_{\mathrm{L}}} \right) \right] \tag{S6}$$

where the normalized concentration of the unbound stress-fibre proteins is $\widehat{N}_{\mathrm{u}} \equiv N_{\mathrm{u}}/N_0$ with $\hat{\eta} \equiv \eta n^{\mathrm{R}}/N_0$, while $\hat{\eta}_{\mathrm{max}}$ is the maximum normalised value of $\hat{\eta}$ corresponding to full occupancy of all available sites for stress-fibres (in a specific direction). Here, $\widehat{N}_{\mathrm{L}}$ is the number of lattice sites available to unbound proteins. The enthalpy μ_{b} of n^{R} bound functional units at steady-state is given in terms of the isometric stress-fibre stress σ_{max} and the internal energy μ_{b0} as

$$\mu_{\mathrm{b}} = \mu_{\mathrm{b0}} - \sigma_{\mathrm{max}} \Omega (1 + \tilde{\varepsilon}_{\mathrm{nom}}^{\mathrm{ss}}), \tag{S7}$$

where Ω is the volume of n^{R} functional units. By contrast, the chemical potential of the unbound proteins is independent of stress and given in terms of the internal energy μ_{u} as

$$\chi_{\mathrm{u}} = \frac{\mu_{\mathrm{u}}}{n^{\mathrm{R}}} + k_B T \ln\left(\frac{\widehat{N}_{\mathrm{u}}}{\pi\, \widehat{N}_{\mathrm{L}}}\right). \tag{S8}$$

For a fixed configuration of the 2D cell (i.e. a fixed strain distribution $\varepsilon_{\mathrm{nom}}(x_i, \varphi)$), the contribution to the specific Helmholtz free-energy of the cell f from the stress-fibre cytoskeleton follows as

$$f_{\mathrm{cyto}} = \rho_0 \left(\widehat{N}_{\mathrm{u}} \chi_{\mathrm{u}} + \int_{-\pi/2}^{\pi/2} \hat{\eta}\, \hat{n}^{\mathrm{ss}} \chi_{\mathrm{b}} d\varphi\right), \tag{S9}$$

where $\rho_0 \equiv N_0/V_{\mathrm{R}}$ is the number of protein packets per unit reference volume available to form functional units in the cell. However, we cannot yet evaluate f_{cyto} as $\widehat{N}_{\mathrm{u}}(x_i)$ and $\hat{\eta}(x_i, \varphi)$ are unknown. These will follow from the chemical equilibrium of the cell as will be discussed in Section 2.1.

The total stress Σ_{ij} within the cell includes contributions from the passive elasticity provided mainly by the intermediate filaments of the cytoskeleton attached to the nuclear and plasma membranes and the microtubules, as well as the active contractile stresses of the stress-fibres. The total Cauchy stress is written in an additive decomposition as

$$\Sigma_{ij} = \sigma_{ij} + \sigma_{ij}^{\mathrm{p}}, \tag{S10}$$

where σ_{ij} and σ_{ij}^{p} are the active and passive Cauchy stresses, respectively. In the 2D setting with the cell lying in the $x_1 - x_2$ plane, the active stress is given in terms of the volume fraction v_0 of the stress-fibre proteins as

$$\begin{bmatrix} \sigma_{11} & \sigma_{12} \\ \sigma_{12} & \sigma_{22} \end{bmatrix} = \frac{v_0 \sigma_{\max}}{2} \int_{-\pi/2}^{\pi/2} \hat{\eta}[1 + \varepsilon_{\mathrm{nom}}(\varphi)] \begin{bmatrix} 2\cos^2\varphi^* & \cos 2\varphi^* \\ \cos 2\varphi^* & 2\sin^2\varphi^* \end{bmatrix} d\varphi, \tag{S11}$$

where φ^* is the angle of the stress-fibre measured with respect to x_2, and is related to its orientation φ in the undeformed configuration by the rotation with respect to the undeformed configuration. The passive elasticity in the 2D setting is given by a 2D specialization of the Ogden (4) hyperelastic model as derived in Shishvan *et al.* (1). The strain energy density function of this 2D Ogden model is

$$\Phi_{\mathrm{C}} \equiv \frac{2\mu_{\mathrm{C}}}{m_{\mathrm{C}}^2}\left[\left(\frac{\lambda_{\mathrm{I}}}{\lambda_{\mathrm{II}}}\right)^{\frac{m_{\mathrm{C}}}{2}} + \left(\frac{\lambda_{\mathrm{II}}}{\lambda_{\mathrm{I}}}\right)^{\frac{m_{\mathrm{C}}}{2}} - 2\right] + \frac{\kappa_{\mathrm{C}}}{2}(\lambda_{\mathrm{I}}\lambda_{\mathrm{II}} - 1)^2, \tag{S12}$$

for the cytoplasm and

$$\Phi_{\mathrm{N}} \equiv \frac{2\mu_{\mathrm{N}}}{m_{\mathrm{N}}^2}\left[\left(\frac{\lambda_{\mathrm{I}}}{\lambda_{\mathrm{II}}}\right)^{\frac{m_{\mathrm{N}}}{2}} + \left(\frac{\lambda_{\mathrm{II}}}{\lambda_{\mathrm{I}}}\right)^{\frac{m_{\mathrm{N}}}{2}} - 2\right] + \frac{\kappa_{\mathrm{N}}}{2}(\lambda_{\mathrm{I}}\lambda_{\mathrm{II}} - 1)^2, \tag{S13}$$

for the nucleus where λ_{I} and λ_{II} are the principal stretches, μ_{C} (μ_{N}) and κ_{C} (κ_{N}) the shear modulus and in-plane bulk modulus of cytoplasm (nucleus), respectively, while m_{C} (m_{N}) is a material constant governing the non-linearity of the deviatoric elastic response of cytoplasm (nucleus). The cell is assumed to be incompressible, and thus throughout the cell, we set the principal stretch in the x_3 −direction $\lambda_{\mathrm{III}} = 1/(\lambda_{\mathrm{I}}\lambda_{\mathrm{II}})$. The (passive) Cauchy stress then follows as $\sigma_{ij}^{\mathrm{p}} p_j^{(k)} = \sigma_k^{\mathrm{p}} p_i^{(k)}$ in terms of the principal (passive) Cauchy stresses σ_k^{p} ($\equiv \lambda_k \partial\Phi_{\mathrm{C}}/\partial\lambda_k$ for the cytoplasm and $\equiv \lambda_k \partial\Phi_{\mathrm{N}}/\partial\lambda_k$ for the nucleus) and the unit vectors $p_j^{(k)}$ ($k = \mathrm{I}, \mathrm{II}$) denoting the principal directions. The total specific Helmholtz free-energy of the cytoplasm is then $f = f_{\mathrm{cyto}} + \Phi_{\mathrm{C}}$ while that of the nucleus is $f = \Phi_{\mathrm{N}}$.

2.1. Equilibrium of the morphological microstate

Shishvan *et al*. (1) have shown that equilibrium of a morphological microstate reduces to two conditions: (i) mechanical equilibrium with $\Sigma_{ij,j} = 0$ throughout the system, and (ii) chemical equilibrium such that $\chi_{\mathrm{u}}(x_i) = \chi_{\mathrm{b}}(x_i, \varphi) = \text{constant}$, i.e. the chemical potentials of bound and unbound stress-fibre proteins are equal throughout the cell. The condition $\chi_{\mathrm{u}} = \chi_{\mathrm{b}}$ implies that $\hat{\eta}(x_i, \varphi)$ is given in terms of $\widehat{N}_{\mathrm{u}}$ by

$$\hat{\eta}(x_i, \varphi) = \frac{\widehat{N}_{\mathrm{u}}\, \hat{\eta}_{\max} \exp\left[\frac{\hat{n}^{\mathrm{ss}}(\mu_{\mathrm{u}} - \mu_{\mathrm{b}})}{k_B T}\right]}{\pi \hat{n}^{\mathrm{ss}} \hat{\eta}_{\max} + \widehat{N}_{\mathrm{u}} \exp\left[\frac{\hat{n}^{\mathrm{ss}}(\mu_{\mathrm{u}} - \mu_{\mathrm{b}})}{k_B T}\right]}, \tag{S14}$$

and $\widehat{N}_{\mathrm{u}}$ follows from the conservation of stress-fibre proteins throughout the cytoplasm, viz.

$$\widehat{N}_{\mathrm{u}} + \frac{1}{V_{\mathrm{C}}}\int_{V_{\mathrm{C}}} \int_{-\pi/2}^{\pi/2} \hat{\eta}\, \hat{n}^{\mathrm{ss}} d\varphi \; dV = 1. \tag{S15}$$

Knowing $\widehat{N}_{\mathrm{u}}$ and $\hat{\eta}(x_i, \varphi)$, the stress Σ_{ij} can now be evaluated and these stresses within the system (i.e. cell and substrate) need to satisfy mechanical equilibrium, i.e. $\Sigma_{ij,j} = 0$. In this case, the mechanical equilibrium condition is readily satisfied as the stress field Σ_{ij} within the

cell is equilibrated by a traction field T_i exerted by the substrate on the cell such that $b\Sigma_{ij,j} = -\mathrm{T}_i$, where $b(x_i)$ is the thickness of the cell in the current configuration. The substrate energy F_{sub} is calculated by applying these tractions to a linear elastic half-space as described in Shishvan *et al*. (1).

The equilibrium free-energy is then given as

$$G \equiv \rho_0 V_{\mathrm{C}} \chi_{\mathrm{u}} + \int_{V_{\mathrm{C}}} \Phi_{\mathrm{C}}\, dV + \int_{V_{\mathrm{N}}} \Phi_{\mathrm{N}}\, dV + F_{\mathrm{sub}} + F_{\mathrm{adh}}. \tag{S16}$$

Here, χ_{u} is given by eq. (S8) with the equilibrium value of $\widehat{N}_{\mathrm{u}}$ obtained from eq. (S15). For the purposes of further discussion, we label the equilibrium value $F_{\mathrm{cyto}} \equiv \rho_0 V_{\mathrm{C}} \chi_{\mathrm{u}}$ as the cytoskeletal free-energy of the cell, and $F_{\mathrm{passive}} \equiv \int_{V_{\mathrm{C}}} \Phi_{\mathrm{C}}\, dV + \int_{V_{\mathrm{N}}} \Phi_{\mathrm{N}}\, dV$ as the passive elastic energy of the cell. Moreover, $F_{\mathrm{cell}} \equiv F_{\mathrm{cyto}} + F_{\mathrm{passive}}$.

2.2. Numerical methods

We employ Markov Chain Monte Carlo (MCMC) to construct a Markov chain that is representative of the homeostatic ensemble. This involves three steps: (i) a discretization scheme to represent morphological microstate (j), (ii) calculation of $G^{(j)}$ for a given morphological microstate (j), and (iii) construction of a Markov chain comprising these morphological microstates. Here, we briefly describe the procedure which was implemented in MATLAB with readers referred to (1) for further details. Typical Markov chains comprised in excess of 2.5 million samples.

In the general setting of a three-dimensional (3D) cell, a morphological microstate is defined by the connection of material points on the cell membrane to the surface of the collagen coated substrate. In the 2D context of cells on collagen coated substrates, this reduces to specifying the connection of all material points of the cell to locations within the collagen coated substrate, i.e. a displacement field $u_i^{(j)}(X_i)$ is imposed on the cell with X_i denoting the location of material points on the cell in the undeformed configuration, and these are then displaced to $x_i^{(j)} = X_i + u_i^{(j)}$ in morphological microstate (j). These material points located at $x_i^{(j)}$ are then connected to material points on the collagen coated substrate at the same location $x_i^{(j)}$, completing the definition of the morphological microstate in the 2D setting.

The cell is modelled as a continuum and thus $u_i^{(j)}$ is a continuous field. To calculate the density of the morphological microstates, we define $u_i^{(j)}$ via Non-Uniform Rational B-splines

(NURBS) such that the morphological microstate is now defined by M pairs of weights $\left[U_L^{(j)}, V_L^{(j)}\right]$ $(L = 1, \dots, M)$. In all the numerical results presented here, we employ $M = 16$ with 4×4 weights $U_L^{(j)}$ and $V_L^{(j)}$ governing the displacements in the x_1 and x_2 directions, respectively. The NURBS employ fourth order base functions for both the x_1 and x_2 directions, and the knots vector included two nodes each with multiplicity four, located at the extrema of the interval. We emphasise here that this choice of representing the morphological microstates imposes restrictions on the morphological microstates that will be considered. Therefore, the choice of the discretisation used to represent $u_i^{(j)}$ needs to be chosen so as to be able to represent the microstates we wish to sample, e.g. the choice can be based on the minimum width of a filopodium one expects for the given cell type. Given $u_i^{(j)}$, we can calculate $G^{(j)}$ using the model described in Section 2.1 with the cell discretised using constant strain triangles of size $e \approx R_0/10$, where R_0 is the radius of the cell in its undeformed configuration.

We construct the Markov chain using the Metropolis (5) algorithm that gives a sequence of random samples from the exponential equilibrium distribution (eq. (S5)). We employ the Metropolis algorithm in an iterative manner so as to enforce the homeostatic constraint (eq. (S3)). The scheme is summarised as follows:

(i) Assume a value of ζ and use the undeformed cell configuration as the starting configuration and label it as morphological microstate $j = 0$ with equilibrium free-energy $G^{(0)}$ calculated as described in Section 2.1.

(ii) Randomly pick one pair of the M weights $U_L^{(j)}, V_L^{(j)}$ and perturb them by two independent random numbers picked from a uniform distribution over the interval $[-\Delta, \Delta]$.

(iii) Compute the new free-energy of this perturbed state and thereby the change in free-energy $\Delta G = G^{(j)} - G^{(j-1)}$.

(iv) Use the Metropolis criterion to accept this perturbed state or not, i.e.
   a. if $\Delta G \leq 0$, accept the perturbed state;
   b. if $\Delta G > 0$, compute $P^{acc} = \exp(-\zeta \Delta G)$ and accept the perturbed state if $P^{acc} > \mathcal{R}$, where $\mathcal{R}$ is a random number drawn from a uniform distribution over $[0, 1]$.

(v) If the perturbed state is accepted, add it to the list of samples as a new morphological microstate, else repeat the configuration prior to step (ii) in the sample list and return to step (ii).

(vi) Keep repeating this procedure until a converged distribution is obtained. Here, we typically use the criterion that the average of $G^{(j)}$ within the generated sample list (labelled $\langle G^{(j)} \rangle$ changes by less than 1% over 100,000 steps of the Markov chain.

(vii) If $\langle G^{(j)} \rangle$ is within $\pm 2\%$ of the homeostatic value of G_s, we accept this distribution, else we modify ζ and repeat from step (i).

2.3. Material parameters

All simulations are reported at a reference thermodynamic temperature $T = T_0$, where $T_0 = 310$ K. Most of the parameters of the model are related to the properties of the proteins that constitute stress-fibres. These parameters are thus expected to be independent of cell type. Notable exceptions to this are: (i) the stress-fibre protein volume fraction v_0; and (ii) the passive elastic properties. Here, we use parameters calibrated for SMCs that give good correspondence with the wide range of measurements reported here. The passive elastic parameters of the cytoplasm are taken to be $\mu_{\mathrm{C}} = 1.67$ kPa, $\kappa_{\mathrm{C}} = 35$ kPa and $m_{\mathrm{C}} = 5$, while the corresponding values for the nucleus are $\mu_{\mathrm{N}} = 3.33$ kPa, $\kappa_{\mathrm{N}} = 35$ kPa and $m_{\mathrm{N}} = 20$ (6–8). The maximum contractile stress $\sigma_{\max} = 240$ kPa is consistent with a wide range of measurements on muscle fibres (9), and the density of stress-fibre proteins was taken as $\rho_0 = 3 \times 10^6\ \mu\mathrm{m}^{-3}$ with the volume fraction of stress-fibre proteins $v_0 = 0.032$. Following Vigliotti *et al*. (3), we assume that the steady-state functional unit strain $\tilde{\varepsilon}^{\mathrm{ss}}_{\mathrm{nom}} = 0.35$ with $\mu_{\mathrm{b0}} - \mu_{\mathrm{u}} = 2.3\, kT_0$ and $\Omega = 10^{-7.1}\ \mu\mathrm{m}^3$. The maximum angular concentration of stress-fibre proteins is set to $\hat{\eta}_{\max} = 1$. The cell in its undeformed state is a circle of radius R_0 and thickness $b_0 = 0.05R_0$, with a circular nucleus of radius $R_{\mathrm{N}} = 10b_0$ whose centre coincides with that of the cell. Results are presented in terms of normalised cell area $\hat{A}^{(j)} \equiv A^{(j)}/A_0$, where $A^{(j)}$ is the area of a morphological microstate (j) while $A_0 = \pi R_0^2$ is the area of the undeformed cell. Thus, we do not explicitly need to specify R_0.

Results are presented for adhesion to incompressible linear elastic substrates with Young's modulus $E_{\mathrm{sub}} = 8\,\mathrm{kPa}, 32\,\mathrm{kPa}$ and a rigid substrate with $E_{\mathrm{sub}} \to \infty$ coated with surface densities of collagen ranging between 6 ng cm^{-2} to 665 ng cm^{-2}. Using a molecular weight of collagen M_{col} of 200 kDa (10) (i.e. 200 kg mol^{-1}) with 1 ligand per molecule, a surface collagen density ρ_{col} of 1 g cm^{-2} corresponds to $3.011\, x10^9$ ligands/cm^2. A range of

ligand densities from $N_{\mathrm{H}} = 175\ \mu\mathrm{m}^{-2}$ to $N_{\mathrm{H}} = 20 \times 10^3\ \mu\mathrm{m}^{-2}$ are analyzed, corresponding to the range of ρ_{col} investigated in the experiments of Engler *et al*. (11). The other parameters of the focal adhesion model are based on commonly accepted ranges; see for example Deshpande *et al*. (12). Specifically, we assumed a uniform surface density of $C_0 = 5 \times 10^3\ \mu\mathrm{m}^{-2}$ of integrin molecules with surface density of integrins sites $C_{\mathrm{r}} = 20 \times 10^3\ \mu\mathrm{m}^{-2}$. The complex stiffness $\kappa_{\mathrm{s}} = \kappa_{\mathrm{p}} = 0.3\ \mathrm{nN}\ \mu\mathrm{m}^{-1}$ while the maximum complex force $\mathrm{F}_{\max} = 0.01\ \mathrm{nN}$ (13).

2.4. Definitions of normalised quantities and observables

Following Shishvan *et al.* (1), the free-energy $G^{(j)}$ can be decomposed as $G^{(j)} = \Upsilon^{(j)} + \Upsilon_0$, where $\Upsilon_0 = \rho_0 V_0 \left[\mu_{\mathrm{u}}/n^{\mathrm{R}} - kT \ln\left(\pi \widehat{N}_{\mathrm{L}}\right)\right]$ is independent of the morphological microstate. It is thus natural to subtract out Υ_0 and define a normalised free-energy as

$$\hat{G}^{(j)} \equiv \frac{\Upsilon^{(j)}}{|G_{\mathrm{S}} - \Upsilon_0|} = \frac{G^{(j)} - \Upsilon_0}{|G_{\mathrm{S}} - \Upsilon_0|}\ , \tag{S17}$$

where G_{S} is the equilibrium free-energy of a free-standing cell (i.e. a cell in suspension with traction-free surfaces). Then, the distribution given by eq. (S6) can be re-written as

$$P_{\mathrm{eq}}^{(j)} = \frac{1}{\hat{Z}} \exp\left[-\hat{\zeta}\hat{G}^{(j)}\right] \tag{S18}$$

with $\hat{Z} \equiv \sum_j \exp\left[-\hat{\zeta}\hat{G}^{(j)}\right]$ and $\hat{\zeta} \equiv \zeta |G_S - \Upsilon_0|$. It then immediately follows that the distributions of states are not influenced by the values of n^{R}, $\widehat{N}_{\mathrm{L}}$ and V_0 and these parameters need not be specified so long as energies are quoted in terms of the normalised energies $\hat{G}^{(j)}$.

Analogously, we define the normalised elastic, cytoskeletal, adhesion, and substrate free-energies of the spread microstate (j) as

$$\hat{F}_{\mathrm{passive}}^{(j)} \equiv \frac{F_{\mathrm{passive}}^{(j)}}{|G_{\mathrm{S}} - \Upsilon_0|}\ , \qquad \hat{F}_{\mathrm{cyto}}^{(j)} \equiv \frac{F_{\mathrm{cyto}}^{(j)} - \Upsilon_0}{|G_{\mathrm{S}} - \Upsilon_0|} \tag{S19}$$

and

$$\hat{F}_{\mathrm{sub}}^{(j)} \equiv \frac{F_{\mathrm{sub}}^{(j)}}{|G_{\mathrm{S}}|}, \qquad \hat{F}_{\mathrm{adh}}^{(j)} \equiv \frac{F_{\mathrm{adh}}^{(j)}}{|G_{\mathrm{S}} - \Upsilon_0|}, \tag{S20}$$

respectively.

For the SMCs with volume $V_0 = \pi R_0^2 b_0$ modelled here, the equilibrium free-standing microstate is a spatially uniform circular cell with $(G_{\mathrm{S}} - \Upsilon_0)/(V_0 k T_0) \approx -4.53\ x\ 10^6\ \mu\mathrm{m}^{-3}$. The free-standing cell is a standard boundary value problem with traction-free boundary

conditions. An iterative FE scheme as described in Shishvan *et al.* (1) is used to solve this boundary value problem and calculate G_S. This solution predicts that the free-standing is circular cell with radius $0.92\ R_0$.

Bibliography

1. Shishvan, S.S., A. Vigliotti, and V.S. Deshpande. 2018. The homeostatic ensemble for cells. Biomech. Model. Mechanobiol. https://doi.org/10.1007/s10237-018-1048-1.
2. Jaynes, E.T. 1957. Information Theory and Statistical Mechanics. Phys. Rev. 106: 620–630.
3. Vigliotti, A., W. Ronan, F.P.T. Baaijens, and V.S. Deshpande. 2016. A thermodynamically motivated model for stress-fiber reorganization. Biomech. Model. Mechanobiol. 15: 761–789.
4. Ogden, R.W. 1972. Large Deformation Isotropic Elasticity - On the Correlation of Theory and Experiment for Incompressible Rubberlike Solids. Proc. R. Soc. A Math. Phys. Eng. Sci. 326: 565–584.
5. Metropolis, N., A.W. Rosenbluth, M.N. Rosenbluth, A.H. Teller, and E. Teller. 1953. Equation of State Calculations by Fast Computing Machines. J. Chem. Phys. 21: 1087–1092.
6. Ronan, W., V.S. Deshpande, R.M. McMeeking, and J.P. McGarry. 2012. Numerical investigation of the active role of the actin cytoskeleton in the compression resistance of cells. J. Mech. Behav. Biomed. Mater. 14: 143–157.
7. Dowling, E.P., W. Ronan, G. Ofek, V.S. Deshpande, R.M. McMeeking, K. a Athanasiou, and J.P. McGarry. 2012. The effect of remodelling and contractility of the actin cytoskeleton on the shear resistance of single cells: a computational and experimental investigation. J. R. Soc. Interface. 9: 3469–79.
8. Dowling, E.P., W. Ronan, and J.P. McGarry. 2013. Computational investigation of in situ chondrocyte deformation and actin cytoskeleton remodelling under physiological loading. Acta Biomater. 9: 5943–5955.
9. Lucas, S.M., R.L. Ruff, and M.D. Binder. 1987. Specific tension measurements in single soleus and medial gastrocnemius muscle fibers of the cat. Exp. Neurol. 95: 142–54.
10. Raj, C. V, I.L. Freeman, R.L. Church, and S.I. Brown. 1979. Biochemical characterization of procollagen-collagen synthesized by rabbit corneal endothelial cells in culture. Invest. Ophthalmol. Vis. Sci. 18: 75–84.
11. Engler, A., M. Sheehan, H.L. Sweeney, and D.E. Discher. 2003. Substrate compliance vs ligand density in cell on gel responses. Eur. Cells Mater. 6: 7–8.
12. Deshpande, V.S., M. Mrksich, R.M. McMeeking, and A.G. Evans. 2008. A bio-mechanical model for coupling cell contractility with focal adhesion formation. J. Mech. Phys. Solids. 56: 1484–1510.
13. Kong, F., A.J. García, A.P. Mould, M.J. Humphries, and C. Zhu. 2009. Demonstration of catch bonds between an integrin and its ligand. J. Cell Biol. 185: 1275–84.

ADDITIONAL FIGURES

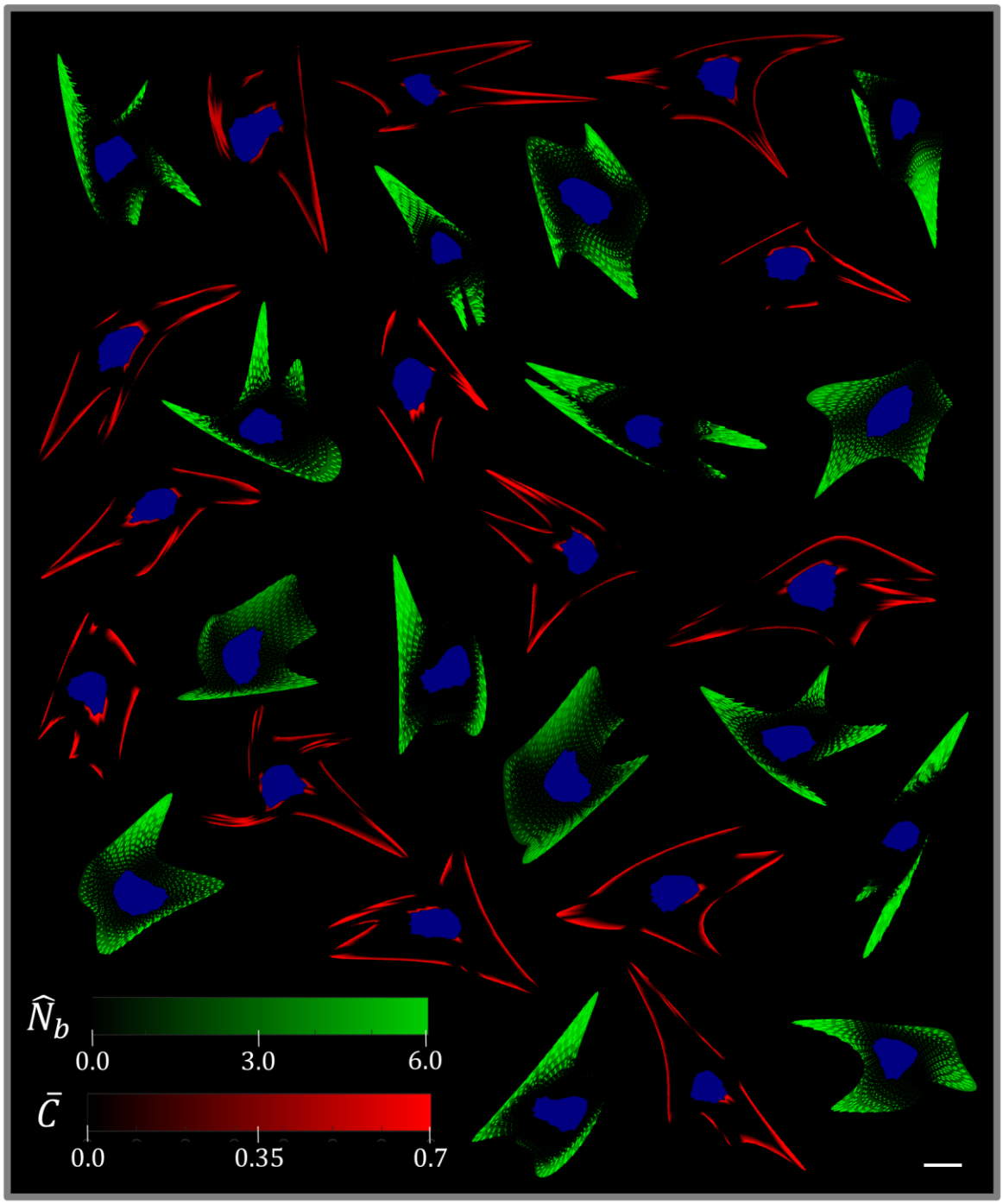

Figure SI-1: Additional configurations of bound stress-fibre protein concentrations $\widehat{N}_b$ (green) with dominant alignment, and focal adhesion distributions $\widehat{C}$ (red). The substrate is rigid, and nucleus is highlighted in blue. The configurations are all from the median of the free-energy $\widehat{G}$ distribution for cells spread on a rigid substrate with a surface collagen density ρ_{col} of 250 ng/cm^2. Scale bar indicates undeformed cell radius R_0.

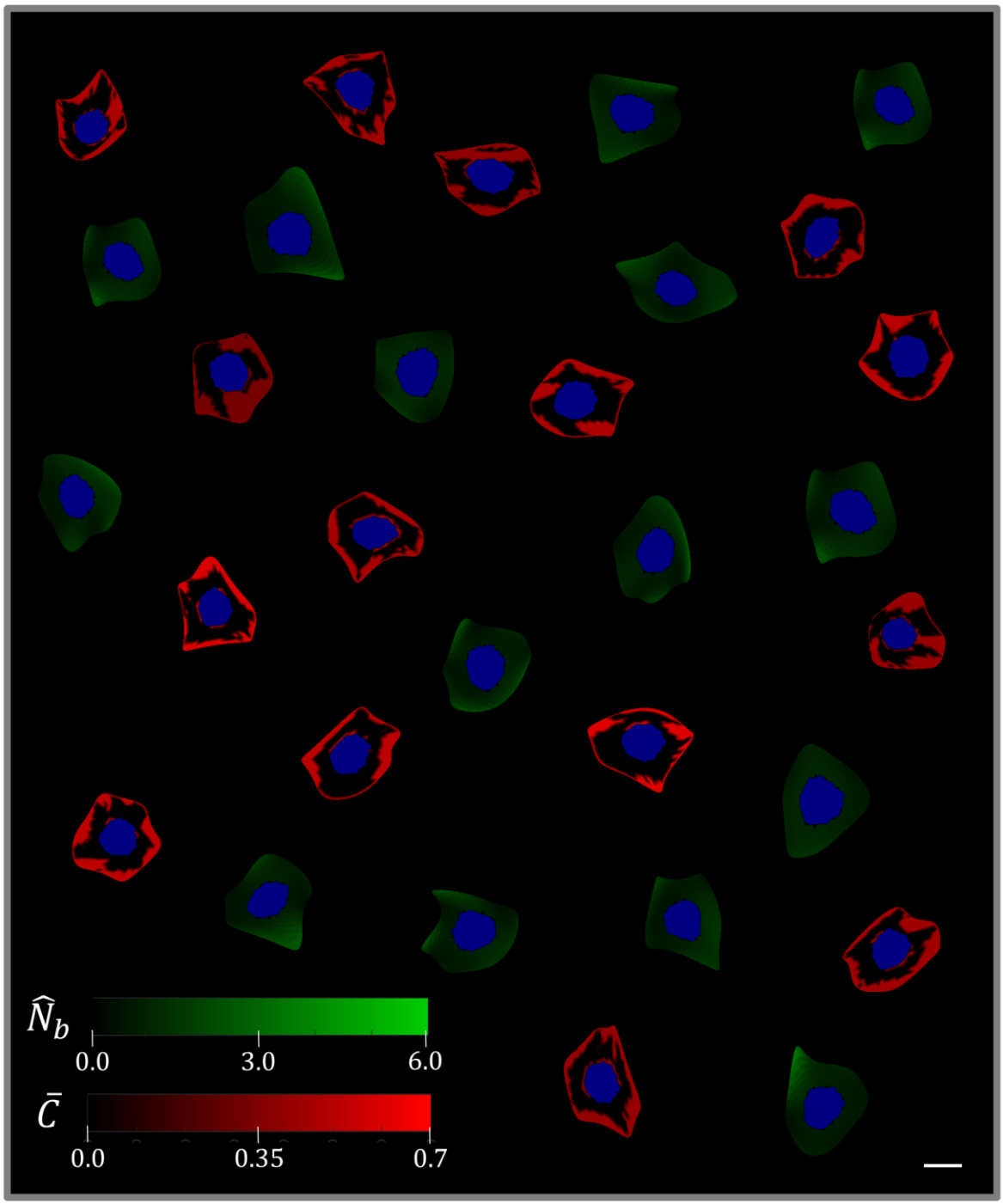

Figure SI-2: Additional configurations of bound stress-fibre protein concentrations $\widehat{N}_\mathrm{b}$ (green), and focal adhesion distributions $\widehat{C}$ (red). The substrate is rigid, and nucleus is highlighted in blue. The configurations are all from the median of the free-energy $\widehat{G}$ distribution for cells spread on a rigid substrate with a surface collagen density ρ_{col} of 6 $\mathrm{ng/cm^2}$. Scale bar indicates undeformed cell radius R_0.

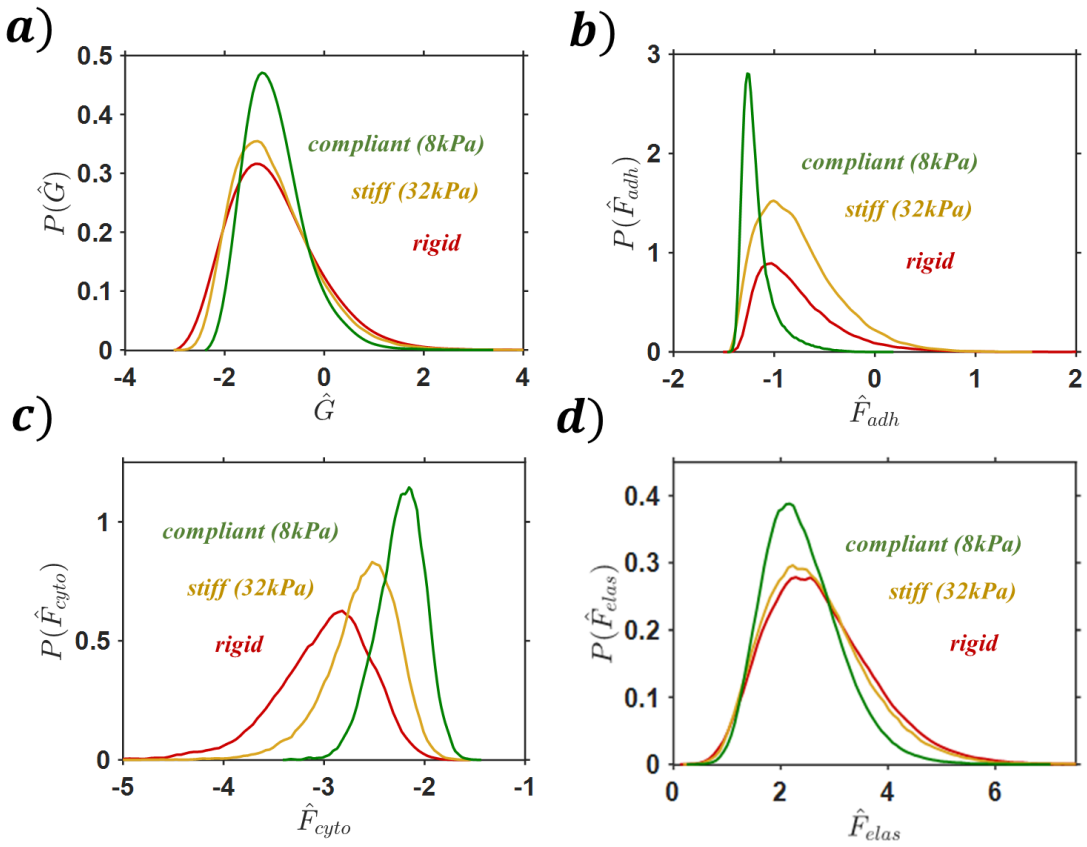

Figure SI-3: Probability density functions for cells spread on substrates of different stiffness at a collagen density of 33 $ng\ cm^{-2}$, of (a) Gibbs free-energy, (b) adhesion free-energy, (c) cytoskeletal free-energy, and (d) elastic free-energy ($\widehat{\boldsymbol{F}}_{\boldsymbol{elas}} = \widehat{\boldsymbol{F}}_{\boldsymbol{passive}} + \widehat{\boldsymbol{F}}_{\boldsymbol{sub}}$).

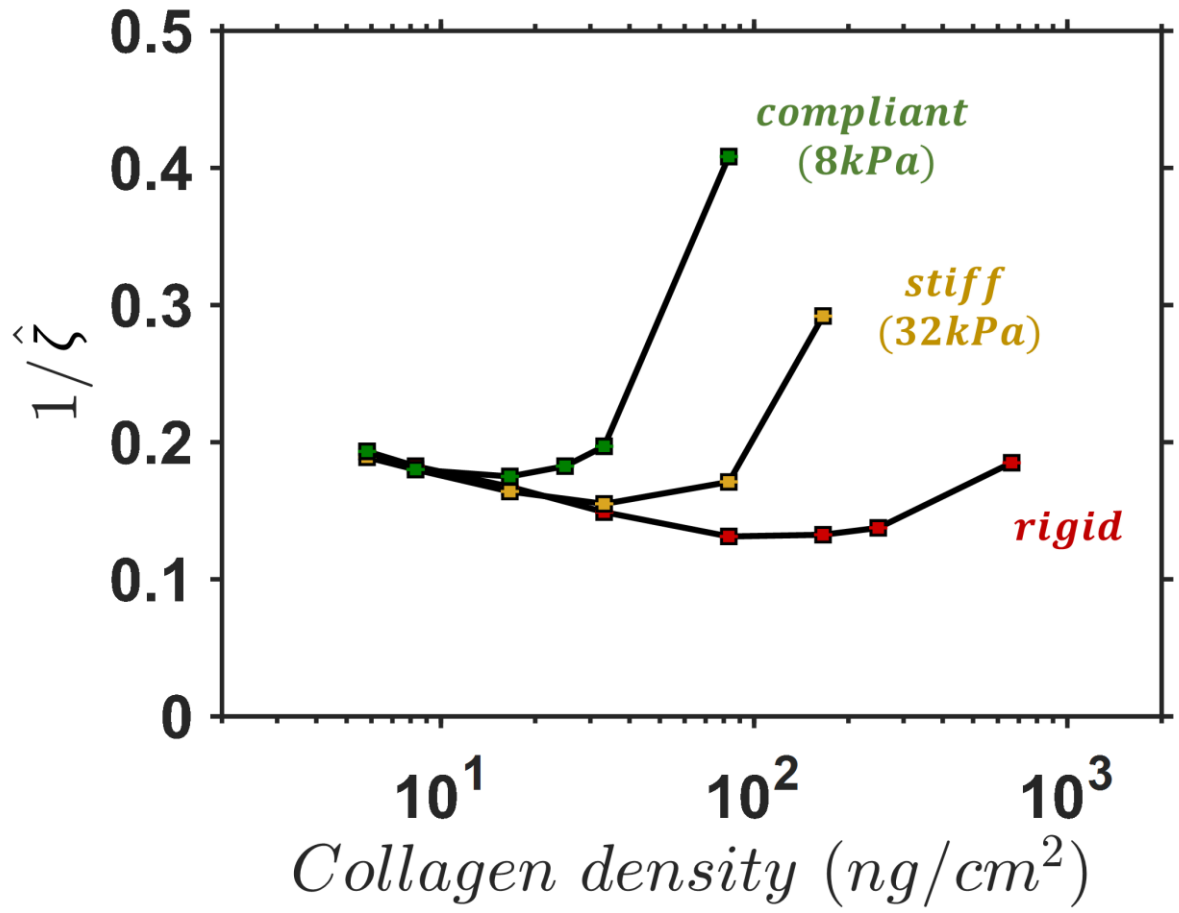

Figure SI-4: Predictions of the normalised homeostatic temperature $1/\hat{\zeta}$.